Temperature dependence of the bulk energy gap in underdoped $Bi_2Sr_2CaCu_2O_{8+\delta}$: Evidence for the mean-field superconducting transition

V. M. Krasnov*
Department of Physics, Stockholm University, AlbaNova University Center, SE-10691 Stockholm, Sweden
(Received 20 February 2009; revised manuscript received 13 May 2009; published 10 June 2009)

Understanding of the puzzling phenomenon of high-temperature superconductivity requires reliable spectroscopic information about temperature dependence of the bulk electronic density of states. Here I present a detailed analysis of the T evolution of bulk electronic spectra in $Bi_2Sr_2CaCu_2O_{8+\delta}$ obtained by intrinsic tunneling spectroscopy on small mesa structures. Unambiguous spectroscopic information is obtained by obviation of self-heating problem and by improving the spectroscopic resolution. The obtained data allow accurate determination of the superconducting transition temperature and indicate that (i) the superconducting transition maintains the mean-field character down to moderate underdoping and is associated with a rapid opening of the superconducting gap, which is well described by the conventional BCS T dependence. (ii) The mean-field critical temperature reaches maximum at the optimal doping and decreases with underdoping. Such behavior is inconsistent with theories assuming intimate connection between superconducting and antiferromagnetic spin gaps and supports proposals associating high-temperature superconductivity with the presence of competing ground states and a quantum critical point near optimal doping.

DOI: 10.1103/PhysRevB.79.214510 PACS number(s): 74.72.Hs, 74.50.+r, 74.25.Jb, 78.67.Pt

I. INTRODUCTION

How does high-temperature superconductivity (HTSC) evolve with decreasing temperature and what happens at the superconducting transition? Where is the real critical temperature T_c? Does HTSC become stronger or weaker upon approaching the undoped antiferromagnetic state? These highly debated questions are crucial for understanding the puzzling HTSC phenomenon. The answers to all those questions could be obtained from the analysis of temperature dependence of the superconducting energy gap $\Delta(T)$ in the quasiparticle (QP) density of states.

So far the majority of spectroscopic studies on HTSC was made by surface-sensitive techniques.[1–7] However, obtaining reliable spectroscopic information from surface spectroscopy on HTSC is immensely difficult: atomic-scale c-axis coherence length, rapid chemical deterioration, presence of the surface states,[4] and inherently different doping state of the surface may preclude determination of bulk electronic properties by surface-sensitive techniques. Furthermore, for $Bi_2Sr_2CaCu_2O_{8+\delta}$ (Bi-2212) the surface spectroscopy probes BiO rather than the superconducting CuO_2 plane.[7] All this urges the necessity of bulk spectroscopy of HTSC.

Intrinsic tunneling spectroscopy (ITS) provides a unique opportunity to probe bulk electronic properties of HTSC. This relatively new technique utilizes weak interlayer (c-axis) coupling in quasi-two-dimensional HTSC compounds, in which mobile charge carriers are confined in CuO_2 planes separated by some blocking layer (e.g., SrO-2BiO-SrO in case of Bi-2212). This leads to the formation of natural atomic-scale intrinsic tunnel junctions and to the appearance of the intrinsic Josephson effect at $T<T_c$.[8–16] ITS is well suited for clarification of questions highlighted above: it is a direct spectroscopic technique, is not sensitive to phase coherence, has very high resolution (neV achievable), is mechanically stable and thus perfectly suited for T-dependent studies of HTSC (unlike surface probe techniques), and, most importantly, probes bulk electronic properties of HTSC.

This work represents a detailed analysis of temperature dependence of the bulk energy gap obtained by ITS on small Bi-2212 mesa structures. Unambiguous $\Delta(T)$ is obtained by careful obviation and cancellation of self-heating. Improved resolution by means of T-differential ITS allows tracing the gap in the phase-incoherent state at $T \gtrsim T_c$. It is observed that at all studied doping levels, the superconducting gap opens in a mean-field manner and is well described by the conventional BCS temperature dependence. The mean-field critical temperature T_c^{mf} decreases with underdoping, thus confronting speculations about persistence of superconductivity up to very high temperatures above T_c in underdoped HTSC. In most underdoped crystals, a remaining weakly T-dependent pseudogap (PG, Δ_{PG}) is observed at $T_c^{mf}<T<T^* \sim 120-150$ K. The pseudogap seems to form a combined gap with the BCS-like superconducting gap below T_c^{mf} and thus competes with superconductivity. No signature of the PG is observed at the optimal doping. The obtained results are inconsistent with theories assuming intimate connection between superconducting and antiferromagnetic spin gaps and support proposals associating HTSC with the presence of competing ground states and a quantum critical point near optimal doping.

In conventional low-temperature superconductors (LTSCs) superconducting transition occurs as a result of the second-order phase transition. It is associated with rapid appearance of the order parameter, represented by the superconducting energy gap $\Delta(T \lesssim T_c^{mf}) \propto \sqrt{1-T/T_c^{mf}}$ and by linear growth of the upper critical field: $H_{c2} \propto \Delta^2 \propto 1-T/T_c^{mf}$. The correlation $H_{c2} \propto \Delta^2$ is fundamental, because H_{c2} is inversely proportional to the square of the coherence length ~ Cooper pair size, which is inversely proportional to the pair coupling energy Δ. All of this is perfectly described by the mean-field BCS-Eliashberg theory of superconductivity.[17]

But how does HTSC emerge with decreasing temperature and what happens at T_c remain unclear. For overdoped cu-

prates, thermodynamic characteristics reveal unambiguous evidence of the second-order phase transition at T_c.[18] Similarly, analyses of Nernst effect,[19] equilibrium[20] and fluctuation[21,22] magnetization and resistivity[23] reveal vanishing of $H_{c2}(T \to T_c)$ in a wide doping range. However, in underdoped cuprates, characterized by the persistence of the normal-state pseudogap at $T > T_c$, the superconducting transition at T_c becomes obscured and both thermodynamic[18] and transport[24] properties become abnormal. According to some reports neither Δ (Ref. 5) nor H_{c2} (Ref. 24) vanishes at T_c, although different interpretations of similar data are possible,[6,21] and vanishing gap at $T \to T_c$ was also reported.[2,25–29]

A related controversy exists about doping dependence of the coupling strength in HTSC. Although T_c and H_{c2} decrease with underdoping,[24,30] the gap measured by surface-sensitive techniques was reported to grow.[1,5] This has been taken as evidence for a continuously increasing superconducting coupling strength $\propto \Delta / T_c$ upon approaching the antiferromagnetic state, assuming an intimate connection between the two states.[31] If true, this would indicate that HTSC has a magnetic origin. However, other experiments reveal the existence of two distinct energy scales, of which one indeed increases with approaching the antiferromagnetic state, while the other follows T_c at all doping levels.[2,25,27–29]

In an alternative scenario, HTSC is facilitated by proximity to a quantum phase transition,[32] which occurs at the quantum critical point at or near optimal doping.[18] In this case superconductivity is strongest at the critical doping level and weakens both in overdoped and underdoped HTSCs.

Does HTSC become stronger or weaker with approaching the antiferromagnetic state? Again, the answer could be obtained by understanding what happens at T_c. If the coupling strength is increasing with underdoping, then so does T_c^{mf}. Some researchers assume that T_c^{mf} may approach room temperature already at moderate underdoping.[5,24,33] To cope with the apparent decrease with underdoping of T_c^{phase}, at which phase coherence is achieved in transport measurements, one has to assume the existence of an extended region $T_c^{phase} < T < T_c^{mf}$ in which the amplitude of the superconducting order parameter is large, but the phase coherence is destroyed by thermal fluctuations.[34]

The extent of the phase-incoherent state $T_c^{mf} - T_c^{phase} \sim G_i T_c^{mf}$ is described by the Ginzburg-Levanyuk parameter G_i.[35] For clean LTSC the fluctuation region is very small because of very small $T_c^{mf}/T_F \sim 10^{-4}$, where T_F is the Fermi temperature.[35] Even for HTSC, $T_c^{mf}/T_F < 0.01-0.1$. Therefore, expansion of the phase-incoherent state well below T_c^{mf} requires $G_i \sim 1$, which can be achieved only by decreasing the dimensionality of the system.[35] Thus one has to assume that superconductivity is either one dimensional (e.g., due to the presence of stripes[31]) or zero dimensional (as in granular superconducting films[36]). In this case, there would be no second-order phase transition nor significant amplitude fluctuations of the order parameter upon establishing of the phase coherence at T_c^{phase}; the superconducting gap would persist at $T_c^{phase} < T < T_c^{mf}$ and could be directly measured by tunneling spectroscopy. Therefore, the knowledge of $\Delta(T)$ close and above T_c^{phase} is crucial for understanding HTSC.

An important clue to understanding temperature evolution of electronic states in HTSC was provided by recent surface photoemission experiments,[3] which, unlike earlier works, showed that Δ does not have a simple d-wave momentum dependence but is described by two distinct energy scales.[2] The antinodal gap has weak temperature dependence at $T \lesssim T_c$ and turns into the pseudogap at $T > T_c$. Furthermore, it increases with underdoping and tends to merge with the insulating gap in the undoped antiferromagnetic state. On the other hand the gap in the nodal "Fermi arc" region must be associated with superconductivity because it follows T_c and vanishes close to T_c at all doping levels. Although those observations are consistent with several previous reports,[27–29] the reliability of surface spectroscopy of HTSC is now under question, because it fails to reveal the electronlike Fermi surface, uncovered by recent quantum oscillation experiments.[37]

The paper is organized as follows. In Sec. II I describe samples and emphasize the dramatic difference between surface and bulk properties of Bi-2212 crystals. Section III contains basic characterization of temperature and size dependencies of ITS on small mesas. In Sec. IV main experimental results on temperature dependence of the bulk gap in Bi-2212 are presented. It is shown that self-heating is effectively obviated by decreasing mesa size and can be simply canceled out from experimental data. The observed results are discussed and summarized in Sec. V. In Appendix A, self-heating and nonequilibrium effects in intrinsic tunnel junctions are analyzed (parts of it were presented in the supplementary material to a letter[38] and included here for completeness). In Appendix B artifacts of in-plane resistance and limitations on the junction size are discussed.

II. EXPERIMENTAL

Interlayer tunneling occurs in various layered HTSC compounds, such as Bi-2212,[15,27,28,39–41] $Bi_2Sr_2CuO_{6+d}$ (Bi-2201),[42] $Tl_2Ba_2CaCu_2O_{8+d}$ (Tl-2212),[43,44] YBaCuO,[45] and some others,[46] as well as in intercalated compounds.[47] ITS was also expanded to non-HTSC layered compounds.[48,49]

Observation of the intrinsic Josephson effect[8] at $T < T_c$ provides the clearest evidence for interlayer tunneling in strongly anisotropic layered HTSC. At present all major fingerprints of the intrinsic Josephson effect were observed, including Fiske[9–11] and Shapiro[10,12] steps in current-voltage characteristics (IVC), the Josephson plasma resonance,[50] thermal activation (TA) (Ref. 13) and macroscopic quantum tunneling[14] from the Josephson washboard potential, and the flux quantization.[9–11,15,16] The latter experiments explicitly confirmed the correspondence between the stacking periodicity of intrinsic Josephson junctions (IJJs) and the crystallographic unit cell of Bi-2212.

Several techniques for preparation of IJJs have been developed, such as patterning mesa structures on top of single crystals,[51] three-dimensional sculpturing by focused ion beam (FIB),[11,15] and double-side fabrication.[12]

Here all measurements were performed on small mesa structures because they are best suited for ITS: they have the best thermal anchoring and are less prone to self-heating and other artifacts, as described in the appendixes. All measure-

TABLE I. Parameters of studied samples: crystal identification with doping level in brackets: OD, slightly overdoped; OP, near optimally doped; UD, moderately underdoped. All samples were made from the same batch of $Bi_2Sr_2Ca_{1-x}Y_xCu_2O_{8+\delta}$ single crystals. N, number of IJJs in mesas; T_c^{onset}, onset of the c-axis resistive transition; T_c^{phase}, appearance of the measurable c-axis critical current and establishing of the c-axis phase coherence; T_c^{mf}, the mean-field critical temperature, obtained from the fit of experimental heating-free $\Delta(T)$; $\Delta_{SG}(0)$, the superconducting gap at $T\rightarrow 0$; Δ_{PG}, the pseudogap at T_c^{mf}; U_{TA}, the c-axis thermal activation barrier in the normal state; $J_c(0)$, the critical current density at $T\rightarrow 0$. For underdoped samples, the first and the second rows represent parameters obtained from fitting of experimental $\Delta(T)$ using BCS T dependence without pseudogap and the combined BCS gap with finite T-independent Δ_{PG} [Eq. (5)], respectively. Note that for both fits T_c^{mf} decreases with underdoping.

Sample	N	T_c^{onset} (K)	T_c^{phase} (K)	T_c^{mf} (K)	$\Delta_{SG}(0)$ (meV)	Δ_{PG} (meV)	U_{TA} (meV)	$J_c(0)$ (A/cm^2)	Reference
S81 (OD)	12		92.5	93	~25	0	15.8	3000	28
SMa (OP)	9	95	91.5	96	33.9	0	25	1000	52
S42 (OP)	9	93.3	92.1	93	33.4	0	22	1100	27
S92 (UD)	34	86	80	90	34.6	0	34	300	38 and 52
			or	87	32.7	12			
S43 (UD)	8	86.5	81.5	90	42.5	0	32.5	510	28
			or	85	38	19			
S82 (UD)	7	78	73	89	46	0	28	270	28
			or	87	44.8	11			

ments were made in the three-probe configuration, which is more robust toward artifacts, as discussed in Appendix B.

A. Samples

To avoid variations caused by different crystal stoichiometries, single crystals from the same batch of Y-substituted $Bi_2Sr_2Ca_{1-x}Y_xCu_2O_{8+\delta}$ [Bi(Y)-2212] were used in this work, with the onset of superconductivity at optimal doping at $T_c^{onset}\simeq 96$ K. Obtained results are not specific for this batch: similar T dependencies were also observed for other crystals by different groups [see, e.g., Refs. 26 and 38–40].

Several mesas of sizes from $\sim 7\times 7$ to $\sim 3\times 3$ μm^2 were patterned simultaneously on each crystal by photolithography and Ar-ion milling. To reduce self-heating, some mesas were trimmed to submicron size by FIB. Details of mesa fabrication are described in Ref. 13. All mesas usually contained the same amount of IJJs N.

Table I summarizes crystals used in this study. To save space and avoid repetitions, I show only a limited amount of raw data and instead address the reader to previous works listed in Table I. All of the studied mesas exhibited good periodicity of QP branches in the IVC, indicating good uniformity of IJJs in the mesas [see the insets in Fig. 2(a) and references in Table I].

The virgin crystals were slightly overdoped with T_c ~91 K. Ar-ion milling provides very uniform and controlled etching but is accompanied by substantial heating at high vacuum. This results in partial out diffusion of oxygen, so that mesas become underdoped. As shown in Ref. 28, underdoping leads not only to decrease in T_c but also to almost linear increase of c-axis resistivity and rapid decrease in the critical current density J_c. Therefore, doping level of crystals was estimated first of all from the analysis of these strongly doping-dependent parameters (as opposed to flat parabolic doping-dependent of T_c near optimal doping). From Table I it is seen that for the studied crystals J_c decreases by 1 order of magnitude from ~3000 A/cm^2 in slightly overdoped crystal S81 to <300 A/cm^2 in moderately underdoped crystals S92 and S82.

The thick solid line in Fig. 1(a) shows a typical resistive transition for a near optimally doped mesa on SMa sample. Here R_0 is the zero-bias resistance measured with small ~1 μA ac. One can see two transitions (three branches) in $R_0(T)$: the major part of the mesa goes into the superconducting state at ~92 K, while the final transition takes place at ~40 K. To clarify their origins, the IVC of this mesa at 4.7 K is shown in the inset of Fig. 1(a).

The IVC consists of multiple branches due to one-by-one switching of IJJs from the superconducting to the resistive (QP) state.[8,27] The number of IJJs N in the mesa can be easily estimated by counting the number of QP branches in the IVC.[41] The branches are strongly hysteretic, that is, switching into the resistive state upon increasing bias occurs at much larger current [~270 μA for the IVC in Fig. 1(a)] than the retrapping current (~2 μA) at which junctions switch back into the superconducting state upon ramping bias down to zero.[13] Such hysteresis is typical for tunnel junctions and is caused by low damping and large specific capacitance of the junctions,[53,54] which allows junctions to remain in the resistive state even below the critical current. Distinct branches in $R_0(T)$ in the superconducting state are originating from different sections of the hysteretic IVC, as indicated by arrows in Fig. 1(a).

Experiments on small mesas allow measurement of the QP resistance at different bias, $R^{QP}(I)$, in the superconducting state,[15,38,51] which is otherwise shunted by the supercurrent.[55] Circles in Fig. 1(a) show the zero-bias QP resistance R_0^{QP} obtained by extrapolation to $I\rightarrow 0$ of the last QP branch with all IJJs in the resistive state. The QP resistance at different biases can be also measured explicitly by first pulsing a current above the critical current I_c and then

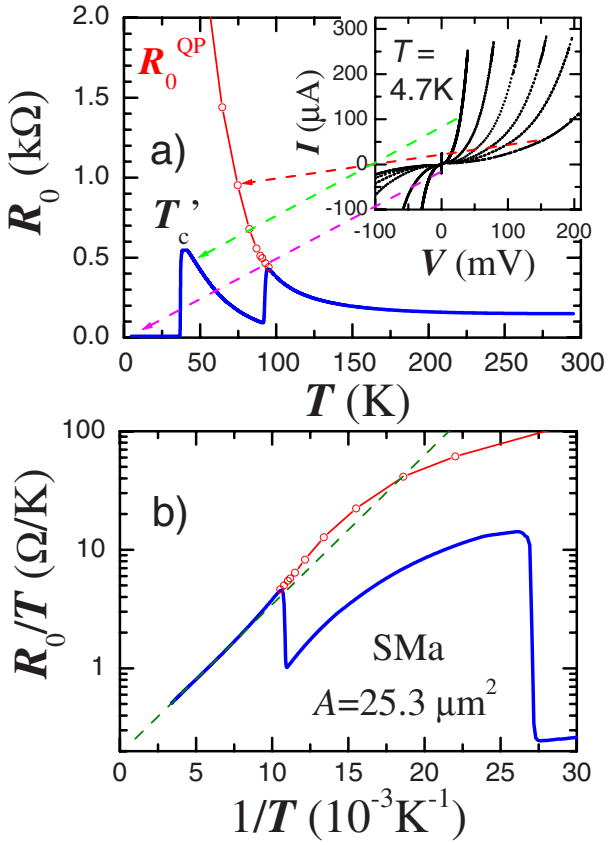

FIG. 1. (Color online) (a) Zero-bias resistance R_0 vs T for a mesa on a nearly optimally doped crystal SMa. Inset shows I-V characteristics at T=4.7 K which clarifies the origin of certain parts of the resistive transition. (b) The same data are shown as a thermal activation plot R_0/T (in a logarithmic scale) vs $1/T$. It is seen that, in the whole normal-state region $T>T_c$, R_0/T is described by the Arrhenius law (dashed line) with a constant TA barrier U_{TA} $\simeq$25 meV.

ramping it down to a desired value.[38] Bias yields an additional parameter for intrinsic tunneling studies, which may render crucial for correct interpretation of the data.[38]

B. Surface versus bulk properties

As seen from the inset in Fig. 1(a), the critical current of the first junction $\sim$20 μA is much smaller than that for the rest of the junctions $I_c\sim$270 μA. This is the top IJJ in the mesa, between the two outmost CuO planes. It is seen that the surface CuO plane is superconducting but has a lower critical temperature $T_c'\simeq$40 K.

Noticeably, the critical current and the QP resistance of the second junction, formed by the second and third CuO planes below the surface, is practically the same as for the rest of the junctions. This unambiguously shows that suppression of superconductivity is solely the surface phenomenon and occurs only in the top CuO plane, and that "bulk" behavior starts already from the second CuO layer below the surface.

The reduction in surface T_c' in our mesas is predominantly caused by chemical deterioration in atmosphere during a short period between cleavage of the Bi-2212 crystal and deposition of the top Au protection layer. Such deterioration was studied in detail in Ref. 56, where it was shown that T_c' could be increased to $\lesssim$80 K if cleavage and deposition are made quickly without breaking vacuum (replicating conditions for surface spectroscopy of HTSC).[2–6] This is still substantially lower than the bulk T_c.

The remaining suppression of T_c' of the surface layer is often attributed to the proximity effect with the electrode. However, I would like to note that although the top CuO layer has a lower T_c' (in some samples less than 20 K) the second layer is perfectly bulk, i.e., not deteriorated with respect to deeper laying layers. Thus, there is no detectable proximity effect between the first and the second CuO layers. This is natural because the transparency of the interlayer barrier is low (prerequisite of the tunnel junction) and the c-axis coherence length is subatomic ($<$0.3 Å). Exactly for the same reasons there should be no considerable proximity effect between the electrode and the top CuO layer, because those are also separated by the blocking BiO layer.

More likely, the suppressed T_c' reflects the fundamental difference between the surface and the bulk, e.g., because the surface is lower doped than the bulk. It should be also noted that even in UHV conditions the chemical deterioration of unprotected Bi-2212 surface is non-negligible. Note that the time of deposition of a monolayer is only $\sim$20 s at the residual pressure $p=10^{-7}$ Torr and even in state of the art surface spectroscopy systems is at best a matter of few hours.

In any case the observed abrupt transition from the surface to the bulk properties within just one atomic layer from the surface clearly indicates that it is not granted that the surface spectroscopy can uncover substantial information about bulk electronic properties of HTSC. All of this urges the necessity of bulk spectroscopy of HTSC, as emphasized in the Introduction.

III. INTRINSIC TUNNELING CHARACTERISTICS OF SMALL MESAS

Figures 2(a) and 2(b) show the c-axis I-V and dI/dV characteristics of a small mesa on the near optimally doped SMa sample at different T. A pronounced kink in I-V (peak in dI/dV), followed by the Ohmic and almost T-independent tunnel resistance is seen.[27] Such the IVC is typical for superconducting tunnel junctions, as demonstrated in Fig. 3(a) and is associated with the sum-gap singularity at $V_{sg}=2\Delta/e$, providing the basis for ITS and opening a possibility to study bulk electronic spectra of HTSC.

Figure 3(a) shows numerically simulated IVCs at T=4.9 and 40 K for a superconducting tunnel junction with a gapless density of states at the Fermi level. The gaplessness was achieved by introducing an appropriate depairing factor Γ =2 meV into the s-wave BCS density of states. Parameters were chosen to fit experimental data for the S42 sample, shown in Fig. 3(c). Clearly, Δ decreased from 33 meV at 4.9 K to 29 meV at 40 K. Figure 3(b) shows the same calculated IVCs in which both current and voltage scales are normalized by the gap. It is seen that the curves merge, because at low $T\lesssim T_c/2$ both V and I scales are $\propto\Delta$. A similar scaling is

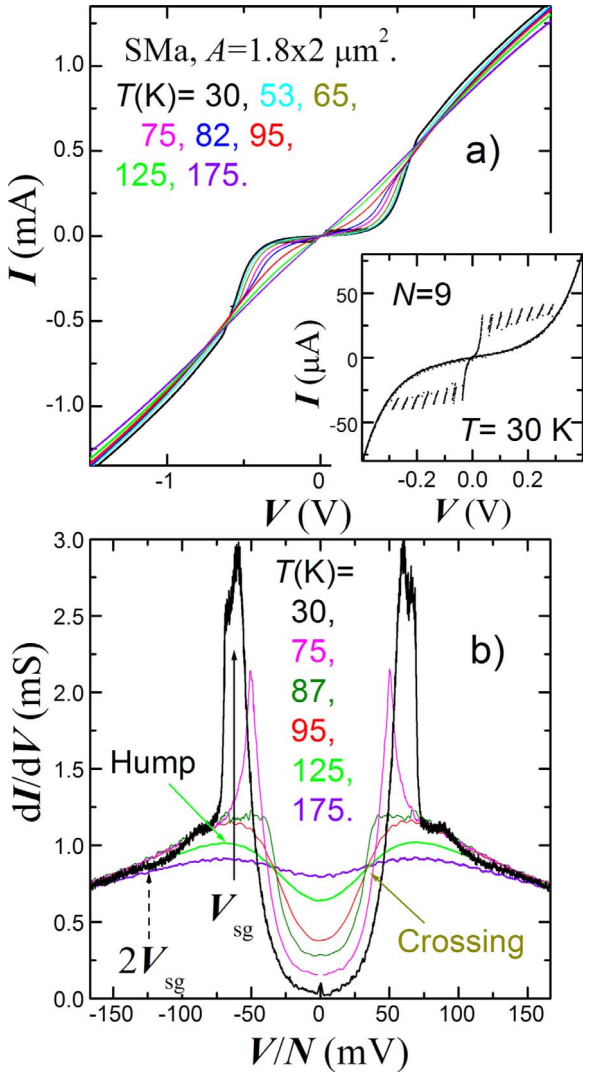

FIG. 2. (Color online) (a) *I-V* curves at different T for a small mesa on a near optimally doped SMa crystal. The kink and transition to approximately Ohmic resistance at the sum-gap voltage is clearly seen. Inset shows multiple quasiparticle branches due to one-by-one switching of intrinsic Josephson junctions into the resistive state. (b) dI/dV vs voltage per junction for the same mesa. Arrows indicate the following characteristic features: the sum-gap peak, a minor double-gap dip at $T<T_c$, and a crossing point and a hump at $T>T_c$.

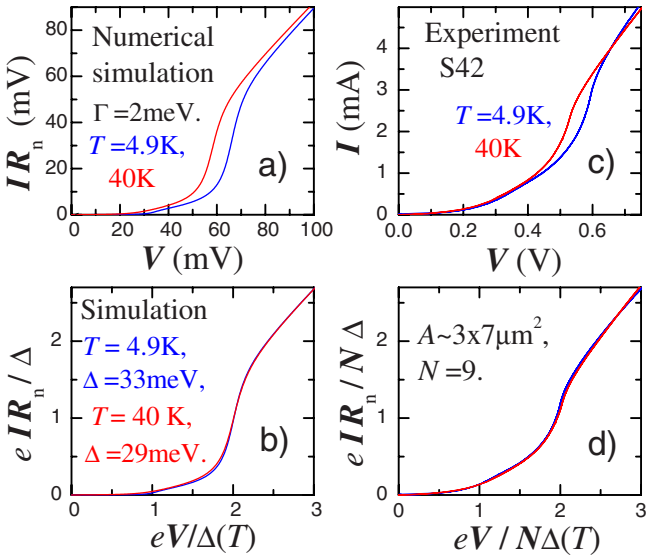

FIG. 3. (Color online) Comparison of (a) simulated and (c) experimental IVCs for S42 at 4.9 and 40 K; (b) and (d) demonstrate collapse of the *I-V* curves, scaled by $\Delta(T)$ and indicate that both V and I scales are determined by $\Delta(T)$.

also observed for experimental data, shown in Fig. 3(d), confirming that the kink is related to the sum-gap singularity (rather than self-heating artifact). Additional arguments can be found in Appendix A, Sec. I.

The sum-gap singularity is not the only gap-related feature in ITS. Further check for self-consistency of our interpretation can be obtained from analysis of additional more subtle gap-related features in dI/dV. The dashed arrow in Fig. 2(b) indicates a small dip at $2V_{sg}$. It was studied in Ref. 41 and was attributed to enhancement of nonequilibrium effects at $eV>4\Delta$, when relaxation radiation of tunneled quasiparticles becomes sufficient for breaking Cooper pairs.

A. Self-heating-free characteristics

It is fair to say that ITS has become a spectroscopic tool as a result of reduction in self-heating. No T-independent Ohmic tunnel resistance, as in Fig. 2(a), could be seen in earlier works,[8,51,57] dealing with large structures. Larger self-heating in such structures leads to development of an acute thermal instability[58] at voltages much smaller than $V_{sg}N$. Another problem in large structures is associated with the limited amount of supercurrent that the CuO plane can carry (see Appendix B). It is interesting to note that exactly the same problems were encountered at the early stage of experimental studies on LTSC tunnel junctions.[59]

In order to obtain unambiguous spectroscopic information, the problem of self-heating has to be carefully addressed. The temperature rise due to self-heating is given by a simple expression[54]

$$\delta T = PR_{Th}(T), \tag{1}$$

where $P=IV$ is the dissipated power and R_{Th} is the effective thermal resistance of the mesa, which is T dependent and, therefore, bias dependent.[52] Detailed analysis of self-heating in ITS, including numerical simulations of distortion of IVCs by self-heating can be found in Appendix A.

In recent years different ways of obviating self-heating in ITS were employed, such as pulse measurements,[39] miniaturization,[52,60] and heat compensation.[40] In Ref. 52 it was emphasized that miniaturization decreases self-heating at a given voltage per junction and provides an unambiguous way for discrimination of artifacts of self-heating (size dependent) from electronic spectra (material property, size independent).

In Figs. 4(a) and 5(a) $dI/dV(V)$ characteristics of large and small mesas on samples S92 (moderately underdoped) and SMa (near optimally doped), respectively, are shown. It is clearly seen how self-heating distorts the last QP branch in

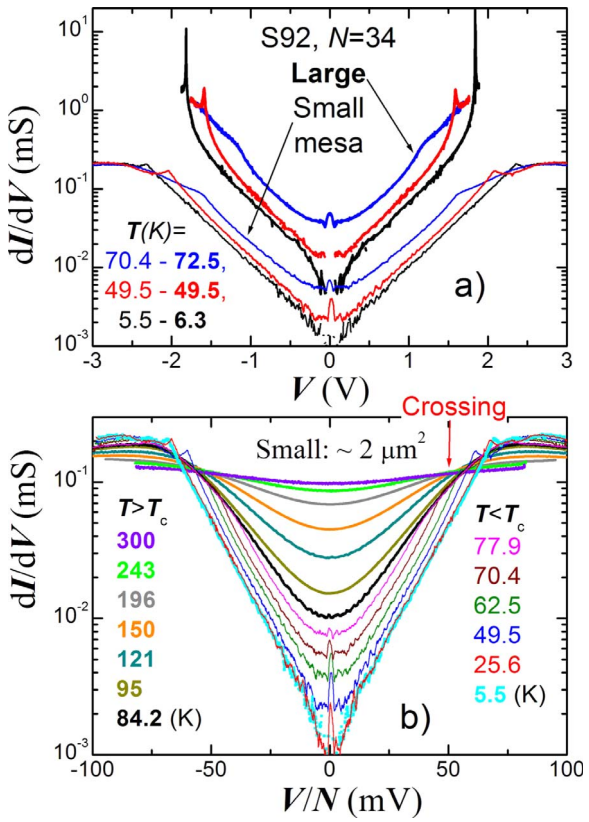

FIG. 4. (Color online) (a) $dI/dV(V)$ (in a semilogarithmic scale) for two mesas with different areas on a moderately underdoped S92 crystal. It is seen how heating and in-plane resistivity bend upward curves at high bias and reduce the sum-gap peak voltage for the large mesa. (b) $dI/dV(V)$ curves at different T for the small mesa. In is seen that the curves maintain the linear V shape (in the semilogarithmic scale) in the whole subgap region when self-heating becomes negligible. A sudden crossover at $T=T_c$ from tunnelinglike with T-independent slope to thermal activation behavior with T-dependent slope is clearly seen. Data are from Ref. 38.

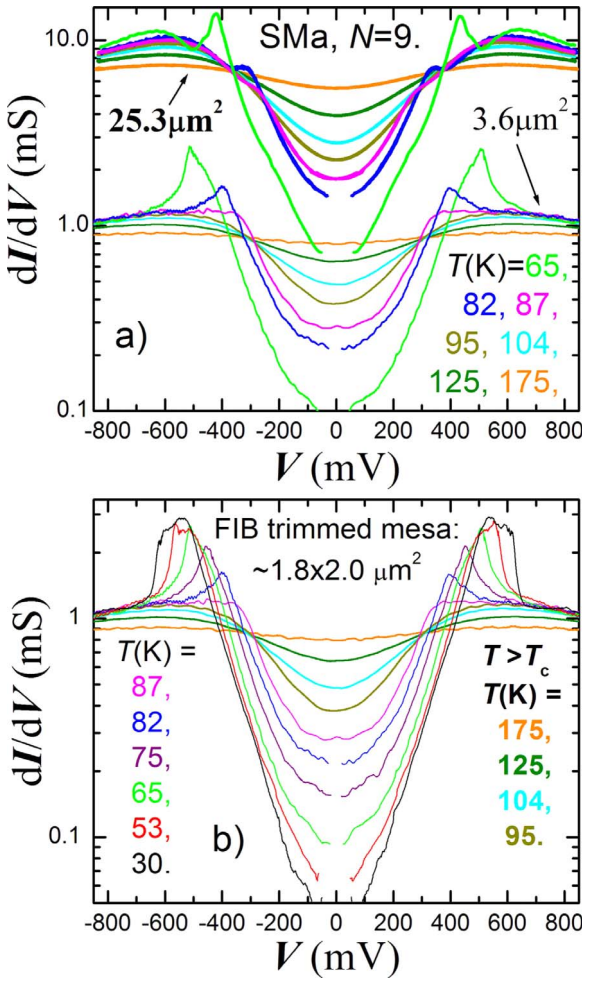

FIG. 5. (Color online) (a) $dI/dV(V)$ (in a semilogarithmic scale) at different T for the same mesas on near optimally doped crystal SMa before and after FIB trimming. The peak voltage is reduced in the larger mesa due to self-heating. (b) dI/dV curves at different T for the small mesa. The characteristic V shape in the semilogarithmic scale is observed at all T. As in Fig. 4, the crossover from T-independent to T-dependent slope occurs at T_c.

large mesas. At low bias, when self-heating is negligible, the characteristics of both mesas are undistorted and the log dI/dV curves remain almost linear and parallel, i.e., simply scale with the mesa area. However, at larger bias log dI/dV in the larger mesas starts to growth faster (superlinear) because the subgap conductance increases with T [see Fig. 2(b)]. The larger mesas also reach the peak earlier, i.e., at lower voltage, as a result of suppression of the gap by T.

Figures 4 and 5(b) show the T evolution of log $dI/dV(V)$ characteristics for the smallest mesas. It is seen that the log dI/dV characteristics for those mesas remain V shaped with almost linear slopes in the whole subgap region $V/N < V_{sg}$, indicating the absence of superlinear distortion by self-heating up to V_{sg}. Insignificance of self-heating for both mesas was explicitly shown in Ref. 52: for SMa by size independence of the peak voltage and for S92 by *in situ* measurement of self-heating. This also follows from the analysis in Sec. IV below.

Note that heating-free ITS characteristics for both crystals have a remarkably trivial V shape in the semilogarithmic scale,[61] and that the slope of the curves for both samples experiences an abrupt crossover from TA-like $1/T$ dependence at $T>T_c$ to tunnelinglike T-independent slope at $T<T_c$. As discussed in Ref. 38, this indicates opening of an additional quantum transport channel for Cooper pairs at $T<T_c$.

B. Thermal-activation behavior in the normal state

In Ref. 38 it was shown that at $T>T_c$ ITS characteristics exhibit TA behavior. Up to moderately high bias $eV<2U_{\mathrm{TA}}$ they are described by a simple expression

$$\frac{dI}{dV}(T,V) \propto \frac{1}{T}\exp\left[-\frac{U_{\mathrm{TA}}}{k_BT}\right]\cosh\left[\frac{eV}{2k_BT}\right], \qquad (2)$$

with a constant TA barrier U_{TA}. Indeed, the cosh term reproduces the rounded V shape of $\log[dI/dV](V)$ curves with the slope that increases as $\simeq 1/T$. The TA behavior at zero bias at $T>T_c$ is demonstrated in Fig. 1(b). In order to expand the

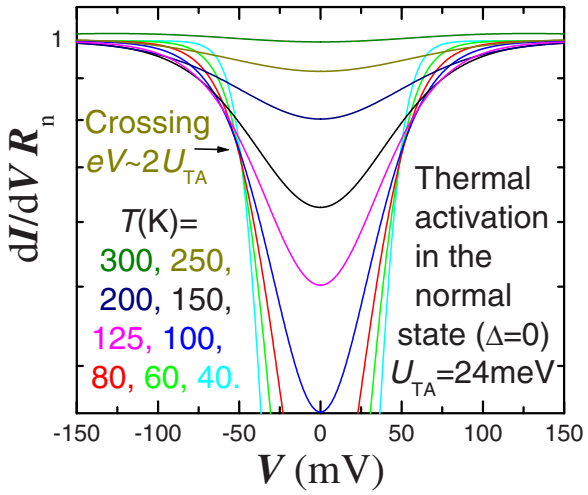

FIG. 6. (Color online) Simulated TA characteristics from Eq. (3) with $U_{TA}=24$ meV. They reproduce all major features of experimental curves at $T>T_c$ in Figs. 4 and 5(b) including the V shape with the slope proportional to the reciprocal temperature and the crossing point at $eV\sim 2U_{TA}$.

TA analysis to higher bias, we have to carefully integrate TA current through the junction

$$I(V)=\int_{-\infty}^{+\infty} t_{TA}(E,V)\rho(E)\rho(E+eV)\{f(E)[1-f(E+eV)] - f(E+eV)[1-f(E)]\}dE. \quad (3)$$

Here $t_{TA}=\exp[-U(E,V)/k_BT]$ is the transition probability of the TA process and U is the effective TA barrier $U(E,V)=\min[(U_{TA}-E-eV/2);0]$, $\rho(E)$ is the density of states in electrodes, and $f(E)$ is the Fermi distribution.

Figure 6 shows simulated $dI/dV(V)$ characteristics (in the semilogarithmic scale) obtained from Eq. (3) with $U_{TA}=24$ meV and for completely normal electrodes $\rho(E)=$const. It reproduces all characteristic features of experimental data at $T>T_c$ in Figs. 4(b) and 5(b), including the crossing point at $eV\simeq 2U_{TA}$ and the inverted parabolic shape at high temperatures $k_BT>U_{TA}$.[28]

Apparently, the c-axis TA barrier should be identified with the phenomenon referred to as the large c-axis pseudogap in the previous literature. However, the amazing success of the trivial TA model, with only one constant parameter U_{TA} in the whole normal region $T>T_c$ and without any momentum-dependent gap in the density of states, suggests that the c-axis pseudogap is most probably not the gap in electronic spectrum of CuO layers, but the property of the blocking BiO layer. Possible "nongap" origins of the c-axis TA barrier were discussed in Ref. 38. Those include resonant tunneling through the impurity state in the blocking layer, inelastic tunneling with excitation of a molecular mode in the barrier, and Coulomb blocking of tunneling in the poorly conducting two-dimensional electron system. As already noted in Ref. 27, the latter bares a striking similarity with experimental V shape characteristics. The Coulomb blocking depends entirely on the conductivity of the two-dimensional electron system, which would naturally explain the increase in TA barrier with underdoping. If so, the TA behavior obscures ITS and should be canceled out from the analysis of spectroscopic features.

C. Improving resolution by T-differential spectroscopy

As seen from Figs. 4 and 5(b), the sum-gap peak in dI/dV is rapidly smearing out with approaching T_c. Remaining weak spectroscopic features can be traced in a standard way by studying higher derivatives, e.g., d^2I/dV^2.[41] However, they are obscured by the parasitic TA background. In Ref. 28 it was shown that the ITS resolution at $T\lesssim T_c$ can be improved by subtracting the TA curve at $T>T_c$. But since TA is strongly T dependent, such subtraction does not completely remove the changing TA background.

Here I suggest the following optimization for TA background cancellation: first, consider a normalized difference between two characteristics as in Figs. 4 and 5(b) at nearby temperatures $T_2>T_1$: $F(T_1,T_2)=\{\ln[dI/dV(T_1)] - \ln[dI/dV(T_2)]\}T_1T_2/(T_2-T_1)$. According to Eq. (2), for pure TA, $F(T_1,T_2)\simeq U_{TA}-eV/2$, i.e., is approximately T independent, thus allowing optimal cancellation of the TA background. Another important advantage of this T-differential scheme is that it emphasizes any T-dependent spectroscopic feature.

In Figs. 7(a) and 8(a) T-differential characteristics $F(T_1,T_2)$ are shown for moderately underdoped crystals S92 and S82, respectively. It is seen that substantially above T_c the curves collapse into a single universal curve, as expected for pure TA. At lower T, the sum-gap peak and the double-gap dip are clearly resolved up to T_c. Interestingly, small deviations from the universal TA curve are seen even above T_c up to ~130 K. To see them more clearly, in Figs. 7(b) and 8(b) the universal TA curves at high $T_{1,2}$ were subtracted from the T-differential characteristics. In such the plot the TA background is completely removed and we can very clearly see the remaining spectroscopic features close and even above T_c.

IV. TEMPERATURE DEPENDENCE OF THE BULK ENERGY GAP

Figures 9–12 summarize temperature dependencies of ITS features for different samples. Data for the same mesas are represented by symbols of the same type and color. Dashed-dotted lines represent the TA barrier, obtained from the zero-bias resistance using Eq. (2): $U_{TA}=k_BT\ln(R_0/T)$. It is seen that U_{TA} is practically constant at $T>T_c$. The sudden fall of U_{TA} marks the superconducting transition.

Crosses in Figs. 10–12 represent crossing points,[38] marked in Figs. 2 and 4(b). In agreement with Fig. 6 they occur at $eV/N\sim 2U_{TA}$. Open symbols in Figs. 9–11 show the hump voltage, marked in Fig. 2(b). It also represents the TA barrier and is roughly T independent at $T>T_c$.[27,28] The hump appears at slightly higher voltage than $2U_{TA}/e$, also in agreement with Fig. 6.

From Figs. 10–12 it is seen that in most underdoped crystals a slight deviation of U_{TA} downwards and the crossing point upward occur with decreasing T below some tempera-

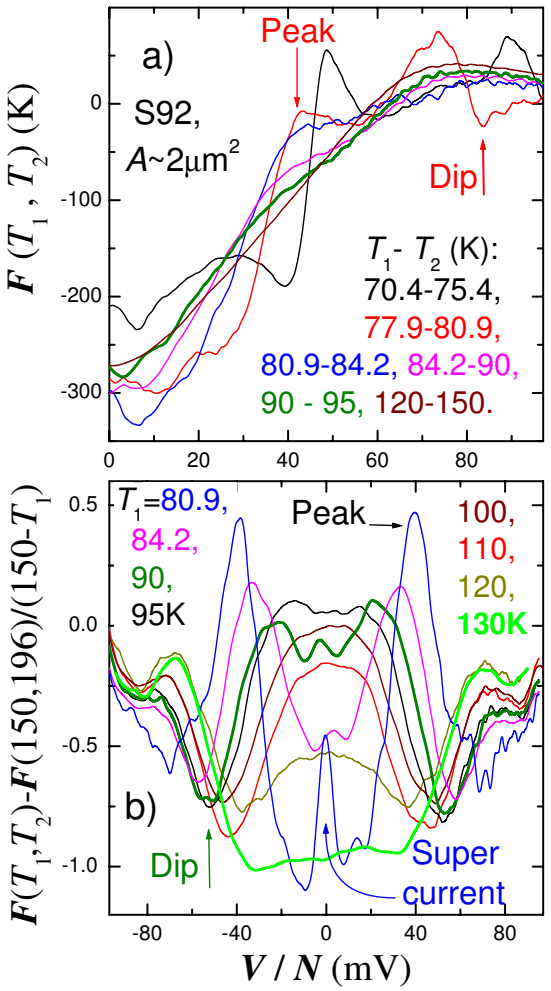

FIG. 7. (Color online) Improvement of spectroscopic resolution at elevated T by means of T-differential spectroscopy for the same small mesa on S92 crystal. In (a) shown are differences between $\ln(\sigma=dI/dV)$ curves from Fig. 4(b) at two consecutive T, normalized by the temperature difference. Such curves emphasize T-dependent spectroscopic features and collapse into the universal curve for the case of TA. In (b) the universal TA curve at high T_1, T_2 was subtracted to remove completely the TA background. This allows clear observation of evolution of the sum-gap peak and the double-gap dip well above the phase-coherent T_c^{phase}.

ture $T^* \sim 130-150$ K. Dashed and dotted vertical lines mark T_c^{phase} and T^*, respectively.

Solid symbols in Figs. 9–12 represent the main experimental result of this work: T dependencies of sum-gap voltages $eV_{sg}/N=2\Delta$. Data points were obtained from the peak and half the double-gap dip in dI/dV (larger symbols) or T-differential characteristics (smaller symbols). The latter allows us to trace the gap up to considerably higher temperatures than before.

In agreement with previous reports[27,28] the bulk gap considerably decreases at $T \to T_c$ for all doping levels. Simultaneously, we observe that the hump also becomes T dependent at $T<T_c$.[28] However, it moves approximately two times slower than the sum-gap peak and is approximately described by the expression $eV_{hump}(T<T_c) \simeq 2U_{TA}+\Delta(T)$. This indicates that the c-axis TA barrier remains intact by the superconducting transition[27] and continue to hinder the QP transport at $T<T_c$.

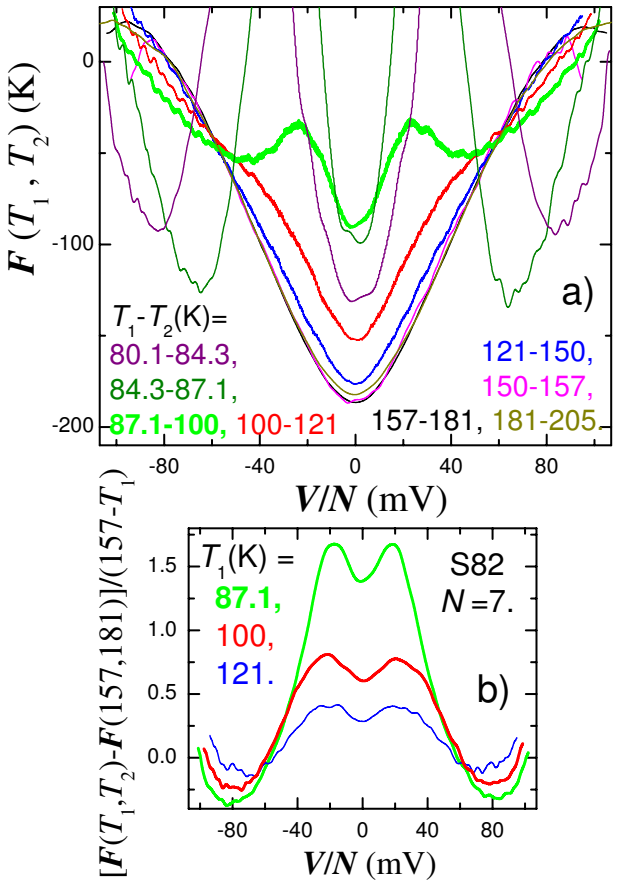

FIG. 8. (Color online) The same as in Fig. 7 for another underdoped S82 crystal. The collapse of curves at high T into the universal TA curve is clearly seen in (a). From panel (b) it is seen that the normal-state pseudogap remains roughly T independent at $T>T_c$.

A. Size dependence

Size dependence of ITS unambiguously reveals the extent of self-heat distortion.[52] Such data are presented in Figs. 9 and 12. Dissipation powers at the sum-gap peak P_{peak} for all studied mesas are shown in insets of Figs. 9(a) and 10–12. P_{peak} scales with the mesa area A.

Solid symbols in Fig. 9(a) show measured V_{sg} for three mesas on the SMa crystal. Size dependence of ITS for this crystal was reported in Ref. 52. It was shown that for mesas with $A<15$ μm^2 the measured gap becomes size independent. Therefore, data for the smallest mesa with $A \simeq 3.6$ μm^2 represent the genuine undistorted bulk gap $\Delta(T)$, as concluded in Sec. III A. The solid line in Fig. 9(a) shows that it is very well described by the conventional mean-field BCS temperature dependence $\Delta_{BCS}(T)$. The same is true for the small mesa on the S92 crystal in Fig. 10(a), which was also identified as heating free in Sec. III A.

Let us now consider the two larger mesas in Fig. 9(a). It is seen that measured gaps become progressively smaller with increasing A and P_{peak}. The observed deviation from the genuine $\Delta(T)$ is perfectly consistent with self-heat distortion,

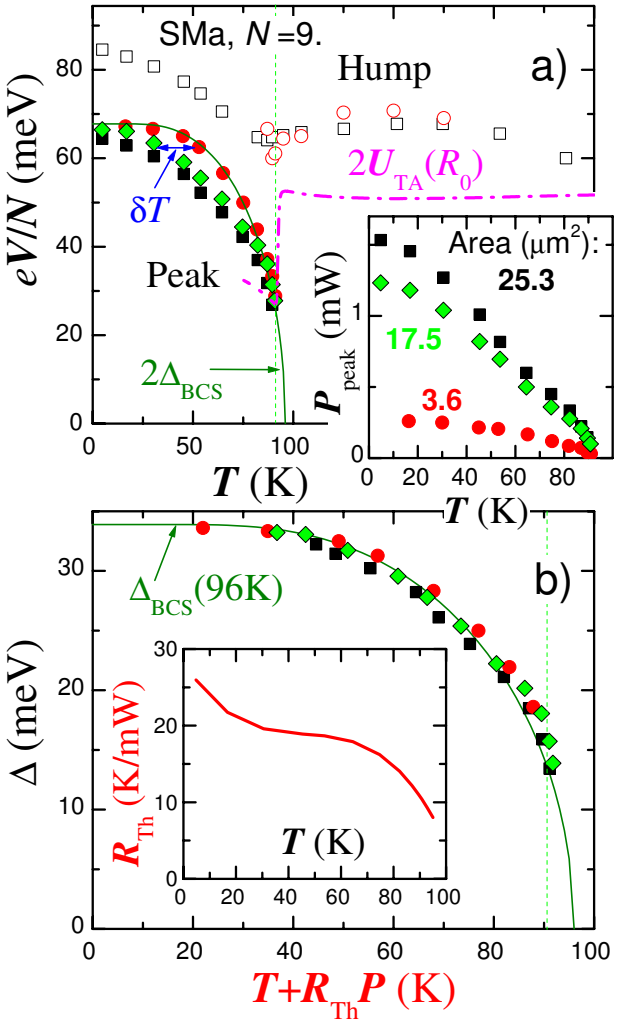

FIG. 9. (Color online) (a) T variation of characteristic spectroscopic features for three mesas on the near optimally doped SMa crystal. Data for the same mesas are shown by symbols of the same type and color. Open symbols, the TA hump; the dashed-dotted curve, $2U_{\mathrm{TA}}$. Downturn of U_{TA} marks the c-axis resistive transition, T_c^{phase}, at which c-axis phase coherence is established. It is marked by the dashed vertical line. Solid symbols, the sum-gap peak; it is seen that the measured gap is distorted with increasing mesa area as a result of self-heating. Inset in (a) shows power at the peak for the same mesas. (b) The heat-compensated T dependence of the bulk energy gap. Solid line shows the conventional BCS T dependence with the mean-field critical temperature T_c^{mf}=96 K. Excellent agreement with experimental data is seen. No pseudogap is observed above T_c^{mf}. Inset in (b) shows the effective thermal resistance for the two larger mesas.

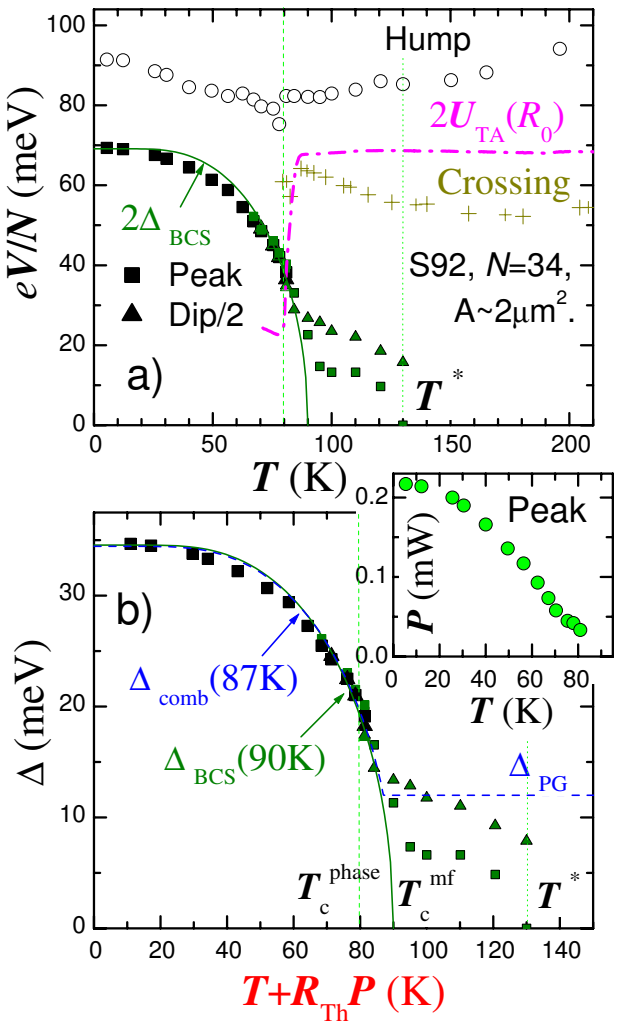

FIG. 10. (Color online) The same as in Fig. 9 for the small mesa on the moderately underdoped S92 crystal. Crosses in (a) represent the crossing point of $dI/dV(V)$ curves at two consecutive temperatures [see Fig. 4(b)]. Filled triangles represent half the double-gap dip. It is seen that signatures of the energy gap (the pseudogap) survive up to $T^* \simeq 130$ K (see Fig. 7). Solid and dashed lines in (b) show that $\Delta(T)$ is equally well described by the pure BCS dependence or the combined gap between the BCS gap and T-independent pseudogap, shown by the dashed line. However, for both fits the mean-field superconducting temperature is smaller than that for the optimally doped crystal in Fig. 9.

as shown in Fig. 15(d). The temperature rise δT is equal to the horizontal shift of the measured gap with respect to the undistorted $\Delta(T)$, as indicated in Fig. 9(a).

Now we can directly calculate the effective thermal resistance of the mesas: $R_{Th}(T)=\delta T/P_{peak}(T)$. The obtained $R_{Th}(T)$ appeared to be approximately the same for both mesas and is shown in the inset of Fig. 9(b). The values of R_{Th} are ranging from ~25 K/mW at 4.2 K to ~10 K/mW at T_c, consistent with direct *in situ* measurements in Ref. 52. Note that in Ref. 52 a separate thermometer was employed for measuring the mesa temperature. Therefore, agreement in obtained $R_{Th}(T)$ in both cases indicates that there is no major thermal gradient along the crystal near the mesa. This is consistent with the conclusion of Ref. 52 that heat transport from the mesa is dominated by ballistic flow of nonequilibrium phonons. In this case the actual heating starts only deep inside the crystal ~l_{ph}—the phononic mean-free path below the mesa, making both heating and in-plane thermal gradient in the mesa small.

The approximate size independence of R_{Th} for the two mesas in Fig. 9 is also consistent with predominantly ballistic heat transport from the mesa. Indeed, from Eq. (4) of Ref. 52 it follows that in this case the thermal resistance becomes size independent for small enough mesas,

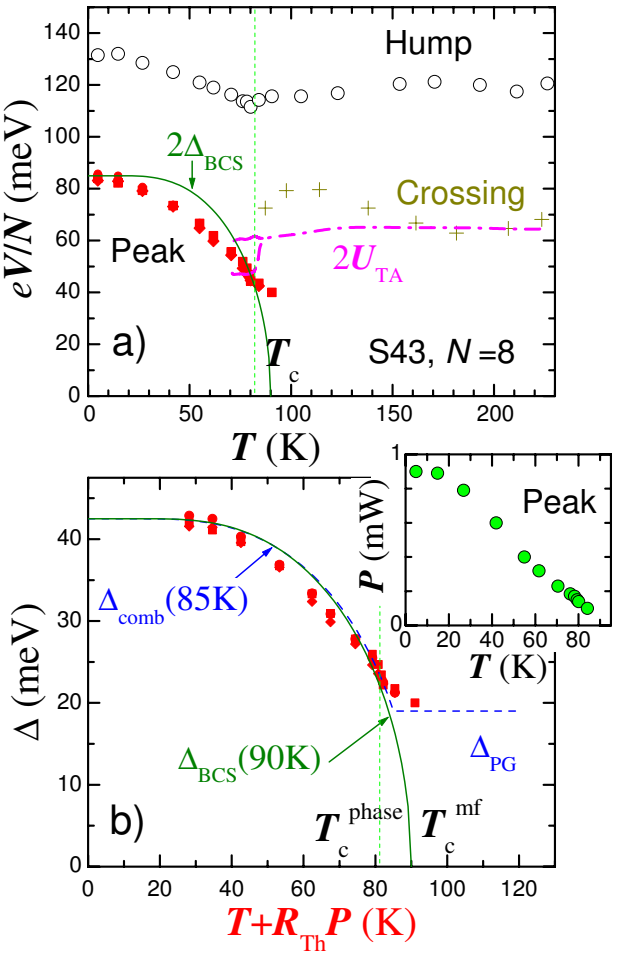

FIG. 11. (Color online) The same as in Fig. 10 for the S43 crystal. It is seen that the superconducting transition even in moderately underdoped HTSC has a mean-field character and is accompanied by opening of the superconducting gap.

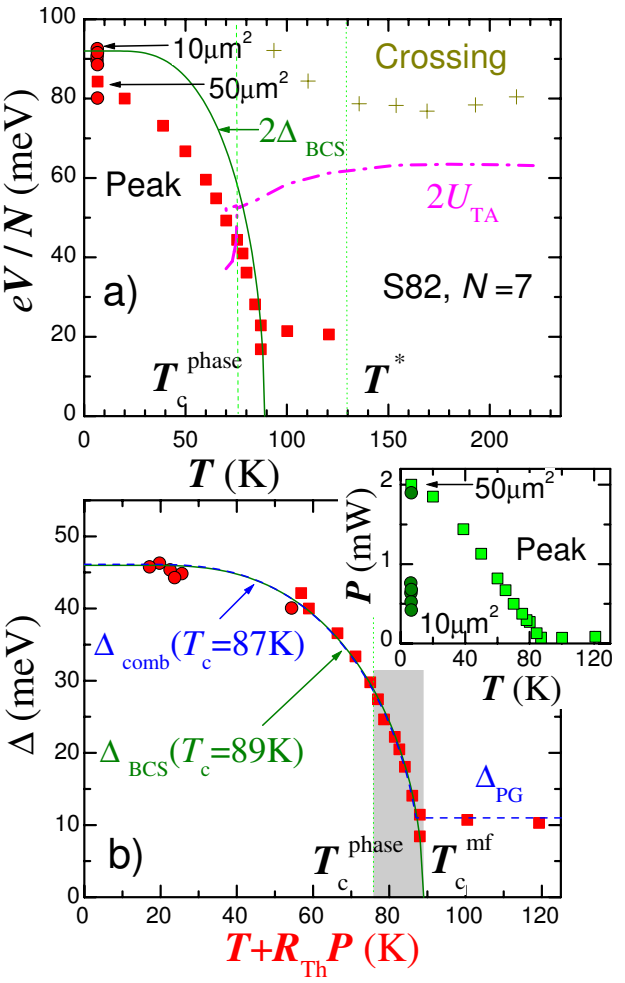

FIG. 12. (Color online) The same as in Fig. 10 for the S82 crystal. Data for mesas with different areas at $T \simeq 6$ K are shown. Gray area in (b) highlights the T region without c-axis phase coherence but with persisting gap and in-plane superconductivity.

$$R_{Th,Ball} \sim (4\pi\kappa_{ab} l_{ph})^{-1}, \tag{4}$$

where κ_{ab} is the in-plane heat conductivity of the crystal.

Of course the thermal resistance of Bi-2212 mesas is not universal and depends on a number of additional factors, as discussed in Appendix A as well as on geometry and materials used in sample fabrication. I want to emphasize that all samples studied here are not only made from the same batch of Bi-2212 crystals (which ensures similar material parameters κ_{ab} and l_{ph}), but they were also made using the same photomask and the same thin-film materials for insulation and electrodes with the same film thicknesses. Also the number of IJJs N in the mesas is similar (except for S92 for which heat compensation is not significant due small heating). Thus, it is reasonable to assume that R_{Th} is similar not only for the two mesas on sample SMa but also for all other mesas studied here. This statement is verified below by analyzing size dependence for the S82 sample in Fig. 12.

B. Self-heat compensation

The knowledge of R_{Th} allows us to recover the genuine T dependence of the gap even for moderately large mesas. In Fig. 9(b) gap values for all three mesas from SMa are plotted as a function of the actual mesa temperature $T_{corr}=T+P_{peak}(T)R_{Th}(T)$, with $P_{peak}(T)$ and $R_{Th}(T)$ from insets in Figs. 9(a) and 9(b), respectively. It is seen that the genuine T dependence of the gap is recovered also for larger mesas after such self-heat compensation. The solid line in Fig. 9(b) shows that the genuine $\Delta(T)$ is perfectly described by the BCS dependence with $T_c^{mf}=96$ K, which is approximately equal to the optimal T_c of our Bi(Y)-2212 crystals. It is close to $T_c^{onset} \simeq 95$ K and slightly higher than the phase-coherent $T_c \simeq 91.5$ K for this crystal, as shown in Fig. 13.

We can also check the self-consistency of the conclusion that ITS characteristics of the smallest mesas on SMa and S92 are not distorted by self-heating. As seen from insets in Figs. 9(a) and 10(b), the maximum P_{peak} for those mesas is ~ 0.2 mW at the lowest T. Therefore, at the lowest T the maximum self-heating δT does not exceed a few K, which does not affect the measured gap. P_{peak} rapidly decreases with increasing T. At $T_c/2$, it reduces by half to ~ 0.1 mW and $\delta T \sim 2$ K. Close to T_c, self-heating becomes negligible even for moderately large mesas. For the smallest mesas from Figs. 9 and 10, $P_{peak}(T \simeq T_c) \simeq 30$ μW and δT is in

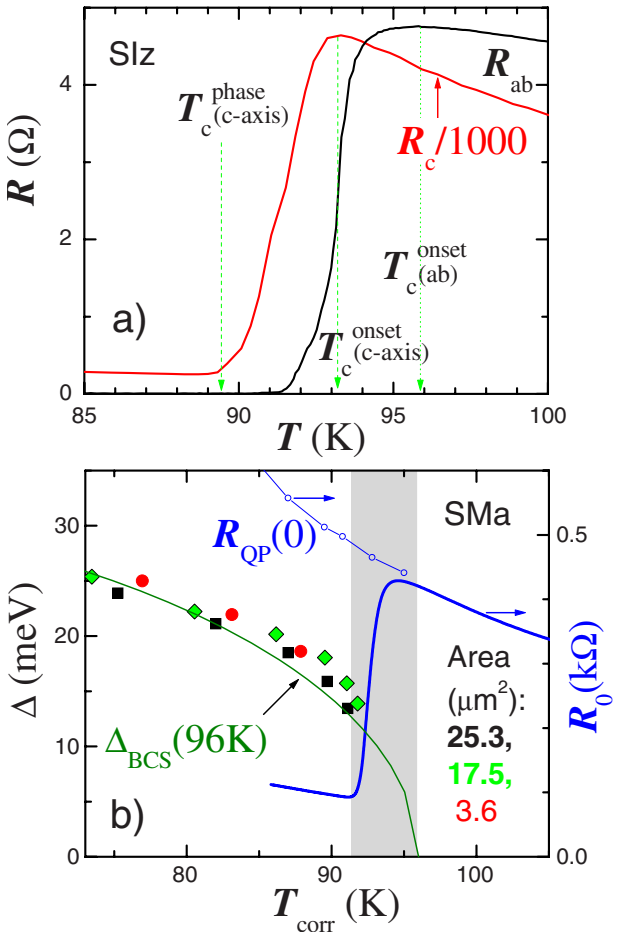

FIG. 13. (Color online) (a) In-plane R_{ab} and c-axis R_c resistive transitions in a slightly underdoped crystal, similar to SMa. Panel (b) reproduces $\Delta(T)$ from Fig. 9(b) along with the resistive transition for a mesa on SMa. It is seen that the onset of in-plane superconductivity coincides with the extrapolated mean-field critical temperature; the onset of c-axis transition is close to the middle of the in-plane resistive transition, while the temperature at which c-axis phase coherence is established is further reduced due to thermal fluctuations. Gray-shaded area in (b) marks the superconducting region without phase coherence in the c-axis direction.

subkelvin. Therefore, the measured gaps for the two smallest mesas are indeed undistorted by self-heating.

Figures 10, 11, and 12(b) represent self-heat compensated $\Delta(T)$ for moderately underdoped mesas. The same $R_{Th}(T)$ was used for self-heat compensation. Collapse of data points for mesas with different area on sample S82 in Fig. 12(b) confirms the applicability of the same $R_{Th}(T)$ for heat compensation. In all cases, the recovered $\Delta(T)$ can be very well described by the mean-field BCS dependence (solid lines) with T_c^{mf} that is larger than T_c^{phase} and close to T_c^{onset}. Those values are summarized in Table I

C. Phase coherence in *c* axis and *ab* plane

In recent years a possibility of persistence of phase-incoherent superconductivity up to very high temperatures above T_c in underdoped HTSC was actively debated. Therefore, it is necessary to clarify the definition of T_c and the difference between c-axis and ab-plane phase coherence.

The c-axis phase coherence is caused by weak Josephson coupling between CuO planes: $E_J=(\hbar/2e)I_c$, where I_c is the total Josephson critical current of the junction. I_c and the Josephson coupling can be easily suppressed by small magnetic fields, which do not affect superconductivity of planes. Moreover, the Josephson coupling can be simply reduced by reducing the junction area. At $T \gtrsim T_J=E_J/k_B \simeq 23.8$ K$(I_c/\mu$A), thermal fluctuations destroy phase coherence and the junction enter in the phase diffusion state with nonzero resistance at zero current.[63,64] Thermal fluctuations also suppress I_c in small mesas.[13,64] Therefore, the c-axis phase coherence in small Bi-2212 mesas is not a material property and should not be confused with a much more robust in-plane phase coherence.

To clarify the difference between in-plane and c-axis phase coherence, in Fig. 13 I show details of corresponding resistive transitions, for the two near optimally doped crystals SIz and SMa. It is seen that the c-axis phase coherence is established at $T_c^{phase} \simeq 89.5$ K. The onset of c-axis transition occurs at $T_c^{onset}(c$ axis$) \simeq 93$ K, which is close to the middle point of the in-plane transition. The onset of ab-plane resistive transition occurs at $T_c^{onset}(ab) \simeq 96$ K, which coincides with the mean-field critical temperature $T_c^{mf} \simeq 96$ K, obtained by extrapolation of $\Delta(T)$ using BCS T dependence, as shown in Fig. 13(b). Shaded areas in Figs. 12(b) and 13(b) indicate regions $T_c^{phase} < T < T_c^{mf}$ in which superconductivity exists without c-axis phase coherence. From Fig. 12(b) it is obvious that the ITS technique works well even without c-axis phase coherence.

The largest lag between T_c^{phase} and T_c^{mf} observed here is 16 K, shaded in Fig. 12(b). In this case such a substantial fluctuation region is due to weak Josephson coupling due to small J_c (see Table I). Importantly, this region occurs always below the optimal T_c and thus should not be confused with claims about precursor superconductivity at much higher T.[5,24]

D. Pseudogap

The main difference between near optimally doped (Fig. 9) and moderately underdoped (Figs. 10–12) crystals is the persistence of some signature of the residual energy gap (the pseudogap Δ_{PG}) at $T > T_c$ up to $T^* \sim 130-150$ K (see Figs. 7 and 8). In the same range $T_c < T < T^*$ we observe an upturn of the crossing voltage and downturn of $U_{TA}(R_0)$ with decreasing T. The pseudogap is seen as deviation from pure TA behavior in a wide bias range in Figs. 7 and 8.

From Figs. 10–12 it is seen that the PG has a much weaker T dependence near T_c^{mf} in contrast to the strong T dependence on the superconducting gap. However, the PG is merging with the superconducting gap at T_c. The overall T dependence both above and below T_c can be described by the combined gap expression,

$$\Delta_{comb}(T) = \sqrt{\Delta_{BCS}^2(T) + \Delta_{PG}^2}, \quad (5)$$

with constant Δ_{PG}. Fits of Eq. (5) to experimental $\Delta(T)$ are shown by dashed blue lines in Figs. 10–12. Below T_c they

are equally good as BCS fits without the PG, but assume lower T_c^{mf}. The corresponding parameters, obtained from fitting the experimental $\Delta(T)$ by pure BCS dependence without PG and by the combined gap expression with constant PG are presented in Table I by the first and the second rows, respectively.

Our present data, together with earlier observation,[27] are consistent with recent angular-resolved photoemission (ARPES) experiments,[2] which demonstrated that the superconducting gap along the Fermi arc closes at T_c at all doping levels, while the gap along antinodal directions (the pseudogap) remains relatively T independent at T_c.

Can this pseudogap be related to superconductivity? The answer is rather straightforward: formation of the combined gap with the superconducting gap indicates that it represents another order parameter, coexisting and competing with superconductivity. Most probably, it represents some sort of charge- and spin-density waves, which were observed in various HTSC compounds.[65] For the S92 mesa the PG is seemingly closing at $T^* \sim 130$ K, as seen from Figs. 7 and 10. However, it should be said that no thermodynamic evidences for the phase transition at T^* were observed so far.[18]

V. DISCUSSION AND CONCLUSIONS

I have shown that technical problems of intrinsic tunneling spectroscopy, such as self-heating (see Appendix A) and in-plane resistance (see Appendix B) can be effectively obviated by reducing mesa size. It is instructive to remind that exactly the same technical problems were encountered at the early stage of experimental studies of conventional LTSC tunnel junctions[59] and were also solved by junction miniaturization, which reduces the area-to-perimeter ratio of the junctions.

I have also shown that self-heating is a trivial phenomenon. It can be easily accounted for and, in case of moderate heating, compensated, so that the genuine $\Delta(T)$ can be recovered. A rule of thumb for "moderate" self-heating is that it should not be obvious in the IVCs: the QP branches should remain periodic and there should be no back bending at V_{sg}. All mesas studied here fall in this category.

The main result of this work is the uncovered genuine T dependence of the bulk energy gap in Bi-2212. For all studied doping levels, $\Delta(T)$ exhibits a strong T dependence, and the superconducting part of it unmistakably tends to vanish in the mean-field BCS manner. For slightly overdoped Bi(Y)-2212 crystals from the same batch, this was shown in Ref. 28. Here I have focused on the underdoped side and have shown that the gap vanishes in the BCS manner also in near optimally doped [Fig. 9(b)] and moderately underdoped (Figs. 10–12) mesas.

Those results are strikingly different from the complete T-independent surface gap, reported in scanning tunneling microscopy (STM) experiments.[5] I want to emphasize that this discrepancy cannot be attributed to self-heating and must find another explanation. Indeed, numerical simulations in Fig. 15 clearly show that the trivial self-heating simply cannot "hide" the qualitative $\Delta(T)$ dependence. For example, there is no way in which one can get the vanishing "measured" (self-heating affected) gap if the true gap is T independent. Furthermore, self-heating becomes insignificant at elevated T because $P_{peak}(T \to T_c^{mf}) \to 0$. On the other hand, STM characteristics behave similar to the T-independent hump feature in ITS, which is the consequence of the c-axis thermal activation barrier. As discussed in Sec. III B, U_{TA} is most likely the property of the blocking BiO plane, which is probed by STM, rather than superconducting CuO planes. The dramatic difference between STM spectra on BiO and CuO surfaces was indeed reported.[7] This highlights the significance of spectroscopic information from bulk CuO planes obtained here.

Good quantitative agreement between T dependence of the BCS and the obtained bulk energy gaps allows unambiguous determination of the "true" mean-field superconducting critical temperature. Indeed, since T_c^{mf} is encoded in the whole BCS $\Delta(T)$, it is determined not just by extrapolation to a hypothetic point of vanishing Δ, but from fitting of the whole $\Delta(T)$, even at low temperatures. I also assume that the good quality of the mean-field BCS fit makes chances for an alternative explanation proportionally less probable, thus providing rather definite answer to the first two questions raised in the Introduction.

The answer for the third question follows from the observed doping dependence of the obtained mean-field critical temperature: from Table I and Figs. 9–12, it is clear that for all studied underdoped samples, T_c^{mf} is in the range 85–90 K, i.e., smaller than the maximum value $T_c^{mf}=96$ K for optimally doped samples. Together with the previous study of slightly overdoped Bi(Y)-2212 crystals from the same batch,[28] this indicates that the true mean-field superconducting critical temperature in Bi-2212 does not continue to increase with underdoping, but reaches maximum at about optimal doping.

Main conclusions that can be drawn from this work are the following:

(i) The superconducting transition, even at moderate underdoping, is predominantly due to conventional mean-field phase transition rather than destruction of phase coherence without amplitude fluctuations. This confronts speculations about persistence of the "precursor" superconducting state in the extended T region above optimal T_c.

(ii) The mean-field superconducting critical temperature reaches maximum at optimal doping and decreases with underdoping. Thus, HTSC does not become stronger with approaching the undoped antiferromagnetic state.

(iii) The pseudogap coexists and competes with superconductivity and disappears near optimal doping.

An important consequence of those conclusions is that high-temperature superconductivity is strongest at optimal doping and becoming weaker with underdoping. This is consistent with the decrease in the upper critical field[30] with underdoping. Therefore, our observations support the idea that the mechanism of HTSC is intimately connected to a quantum critical point near optimal doping,[18,32] rather than closeness to the antiferromagnetic state.[31]

ACKNOWLEDGMENTS

I am grateful to A. Yurgens, for providing Bi(Y)-2212 crystals; to I. Zogaj, M. Sandberg, and A. Yurgens for assistance at early stage of this work; and to S. O. Katterwe and A. Rydh for useful discussions. Financial support from the K. & A. Wallenberg foundation, the Swedish Research Council, and the SU-Core Facility in Nanotechnology is gratefully acknowledged.

APPENDIX A: ANALYSIS OF SELF-HEATING IN ITS

Despite relative simplicity of self-heating phenomenon (it is certainly the most trivial problem in HTSC spectroscopy), discussion of self-heating in ITS has caused a considerable confusion, a large part of which has been caused by a series of publications by Zavaritsky,[66] in which he "explained" the nonlinearity of ITS characteristics by assuming that there is no intrinsic Josephson effect. Irrelevance of that model for ITS was discussed in Ref. 67.

A certain confusion might be also caused by a large spread in thermal resistances, R_{Th}, reported by different groups.[52,57,68,69] For the sake of clarity it should be emphasized that those measurements were made on samples of different geometries. It is clear that R_{Th} depends strongly on the geometry[52,60] and is much larger in suspended junctions with poor thermal link to the substrate[69] than in the case when both top and bottom surfaces of the junctions are well thermally anchored to the heat bath.[40] For mesa structures similar to those used in this study (a few μm in-plane size, containing $N \simeq 10$ IJJ), the R_{Th} was consistently evaluated by different techniques as $R_{Th}(4.2\ \mathrm{K}) \sim 30-70\ \mathrm{K/mW}$ (depending on bias)[52,68] and $R_{Th}(90\ \mathrm{K}) \sim 5-10\ \mathrm{K/mW}$.[52] Larger values $R_{Th} > 100\ \mathrm{K/mW}$ which might be inferred from Ref. 57 are unrealistic for our mesas because they can withstand dissipated powers in excess of 10 mW without being melted.

Yet, R_{Th} of mesas is not universal and may depend on the geometry, materials used for sample fabrication, and the heat transport mechanism. In case of heat diffusion, the resistance for heat flow into the pedestal for small enough mesas is[52]

$$R_{Th,Diff} \simeq (4\sqrt{\kappa_{ab}\kappa_c}a)^{-1}. \quad \text{(A1)}$$

Here $\kappa_{ab,c}$ are heat conductivities along the ab plane and in the c-axis direction, respectively, and a is the radius of the mesa. For ballistic heat flow it is approximately size independent (for $a < l_{ph}\sqrt{\kappa_{ab}/\kappa_c}$) and is given by Eq. (4). The parallel heat conductance channel through the top electrode should also be added [see Eq. (7) in Ref. 60].

Spectroscopic features in IVCs of IJJs with different areas A occur at specific area-independent power densities q. For example, the sum-gap singularity occurs at $q \simeq 4\Delta^2/(e^2\rho_c s)$, where ρ_c is the c-axis resistivity and s is the interlayer spacing. However, the total power, $P=qA$ decreases with decreasing area. Therefore, reduction in mesa sizes provides a simple way for reduction in self-heating.[60] Consequently, variation in dI/dV characteristics with the junction size and geometry provides an unambiguous way of discriminating artifacts of self-heating from the spectroscopic features.[52]

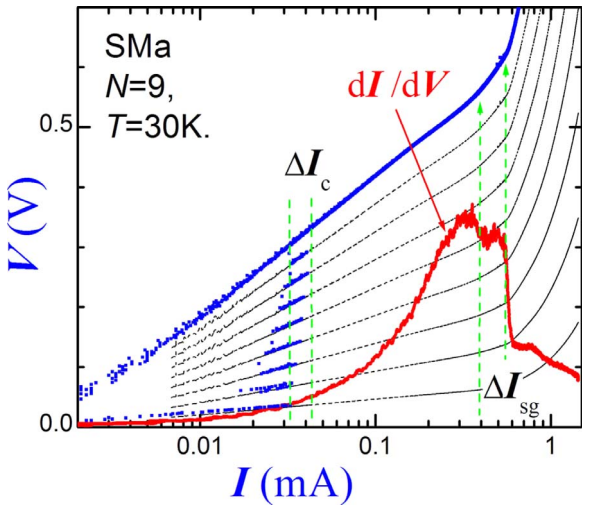

FIG. 14. (Color online) The IVC at $T=30$ K from Fig. 2 in a semilogarithmic scale. Thin lines are multiple integers, indicating good periodicity of quasiparticle branches. However, a small nonuniformity of the junctions is seen from the spread of critical currents ΔI_c, which leads to splitting ΔI_{sg} of the sum-gap peak in $dI/dV(I)$ (red line) because different junctions reach V_{sg} at slightly different currents.

1. Peak splitting in nonuniform junctions

As discussed in Ref. 67, atomic separation between IJJs precludes any substantial temperature difference between them. Thus, all junctions in a mesa warm up synchronously and there may be only one collective artifact of heating for all IJJs in the mesa. To the contrary, if the peak is the sum-gap singularity, it is an individual property of each IJJ. If junctions are not perfectly identical, the peak in dI/dV will split in up to N subpeaks. Indeed, peak splitting is quite often observed in experiment and was already reported in Ref. 62 along with supporting numerical simulations.

In Fig. 14 the IVC at $T=30$ K from Fig. 2 is replotted in a semilogarithmic scale V vs ln I. As discussed in Ref. 38 the IVC becomes nearly linear on such a scale. Thin lines are multiple integers of the last branch divided by $N=9$. Coincidence of those with quasiparticle branches indicates good periodicity of the latter. However, a minor nonuniformity is observed as a gradual increase in I_c with the brunch number. The total spread of the critical current ΔI_c from the second to the last IJJ is marked in the figure. The red line shows $dI/dV(I)$ for the same IVC. A small splitting of the peak ΔI_{sg} is seen. Thus, the peak is not a collective phenomenon of the whole mesa but is a genuine characteristic of each individual IJJ. From Fig. 14 it is seen that ΔI_{sg} has approximately the same width in the logarithmic scale as ΔI_c. Therefore the splitting is proportional to the difference in critical currents of IJJs in the mesa and is due to the corresponding spread in currents I_{sg} at which individual junctions reach V_{sg}. Thus, nonuniformity of junctions, although usually unwanted for ITS, helps to understand the origin of the peak in ITS characteristics of small Bi-2212 mesas.

2. How self-heating affects I-V characteristics

How self-heating *can* distort the IVCs of Josephson junctions is obvious: since self-heating rises the effective T, it

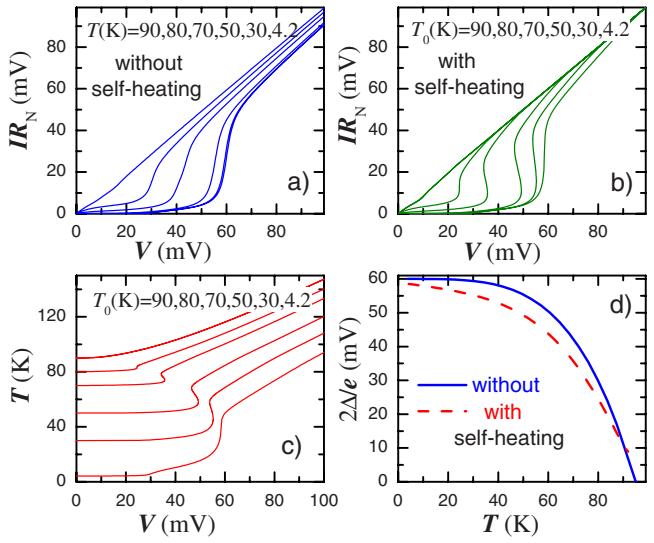

FIG. 15. (Color online) Simulated distortion of superconductor-insulator-superconductor (SIS) tunneling characteristics by strong self-heating. (a) Undistorted IVCs at different T. Simulations were made for typical parameters of our mesas, including detailed $\kappa(T)$ for Bi-2212 and for coherent directional d-wave tunneling. (b) Distorted IVCs at the same base T. (c) The mesa temperature as a function of bias. (d) T dependence of the genuine superconducting gap (solid line) and the "measured" gap obtained from distorted IVCs (dashed curve). Note that even strong self-heating (T reaches $T_c/2$ at V_{sg} at 4.2 K) does not cause considerable distortion of the measured gap. Data are from Ref. 62.

may affect the IVC only via T-dependent parameters. There are three such parameters: (i) the quasiparticle resistance, (ii) the superconducting switching current, and (iii) the superconducting gap. They will affect the IVC of mesas, containing several stacked IJJs, in the following manner.

The consecutive increase in T upon sequential switching of IJJs from the superconducting to the resistive state will distort the periodicity of quasiparticle branches. Each consecutive QP branch will have a smaller QP resistance (smaller V at given I) and smaller switching current. This type of distortion becomes clearly visible (at base $T=4.2$ K) when $\delta T \gtrsim 20$ K.[60,67]

For better understanding of the influence of self-heating on IVCs of Josephson junctions, in Fig. 15 I reproduce the results of numerical simulation of such the distortion, made specifically for the case of Bi-2212 mesa with the corresponding T-dependent parameters (see Ref. 62 for details). Figure 15(a) shows a set of undistorted IVCs at different T for coherent directional d-wave tunneling with some trial $\Delta(T)$, shown by the solid line in Fig. 15(d). Panels (b) and (c) show the distorted IVCs and the actual junction temperature, respectively. It is seen that combination of self-heating and T dependence of Δ may lead to appearance of back bending of the IVC at the sum-gap knee. The dashed line in panel (d) represents the measured gap obtained from the peak in distorted dI/dV characteristics. Remarkably, the deviation from the true $\Delta(T)$ is marginal, despite large self-heating, $\Delta T \simeq T_c/2$ at 4.2 K. Numerical simulations have shown that even self-heating up to T_c at the sum-gap knee does not cause principle changes in the behavior of the measured gap. The robustness of the measured gap with respect to self-heating is due to the flat T dependence of the superconducting gap at $T<T_c/2$ and to simultaneous vanishing of dissipation power at V_{sg} together with $\Delta(T)$ at $T \to T_c$, as shown in insets of Figs. 9–12.

3. Heating or nonequilibrium phenomena?

Finally, it is important to emphasize that the concept of heat diffusion is inapplicable for small Bi-2212 mesas containing only few atomic layers. The phonon transport in this case is ballistic[52,70] and the energy flow from the mesa is determined not by collisions between the tunneled nonequilibrium QPs with thermal phonons, but by spontaneous emission of a phonon upon relaxation of the nonequilibrium QP.[41] This process is not hindered at $T=0$. Therefore, the effective R_{Th} (and self-heating) can be much smaller because it is not limited by poor thermal conductivity at $T=0$ but is determined by the fast almost T-independent nonequilibrium QP relaxation time. The concept of self-heating becomes adequate only in the bulk of the Bi-2212 crystal, where the dissipation power density and the temperature rise are much smaller due to the much larger area of the crystal. For more details see the discussion in Ref. 52. The nonequilibrium energy transfer channel is specific for atomic-scale intrinsic Josephson junctions made of perfect single crystals. It can explain a remarkably low self-heating at very high bias.[41]

APPENDIX B: ARTIFACTS OF IN-PLANE RESISTANCE

In experiments on large mesas[57] or suspended structures,[69] no clear Ohmic tunneling resistance could be observed. Instead a negative differential resistance (acute back bending) progresses at high bias. Similar behavior is also observed for moderately large mesas, when measurements are made in the four-probe configuration.[71] This is in stark contrast to three-probe measurements on small mesas reported here [see Fig. 2 and Refs. 27, 28, 47, and 52].

The continuous negative resistance is not described by self-heating in tunnel junctions because those should always reach the T-independent positive tunnel resistance at high bias. Thus self-heating is not the primary cause of the acute back bending. Rather, the negative differential resistance observed in large structures is caused by the loss of equipotentiality of CuO planes upon which the measurement of IVCs in mesa structures is relying. The latter can be triggered by development of a hot spot[58] but can even occur without self-heating due to in-plane resistive transition of CuO planes when the applied current exceeds the critical current of the CuO plane.[71]

1. Acute back bending without heating and the difference between three- and four-probe measurements

Here I demonstrate how acute and not recovering back bending develops in the IVC of the mesa as a result of the finite in-plane resistance and without any self-heating. I also explain the difference between four-probe measurements that

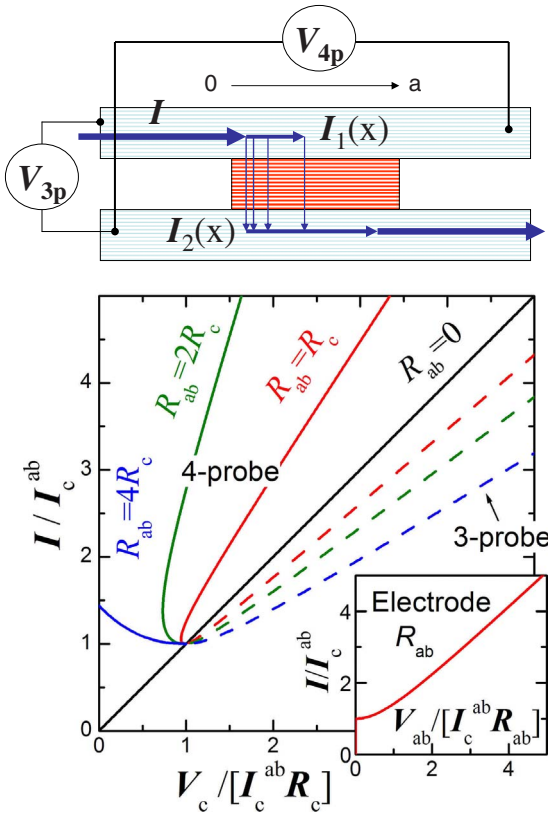

FIG. 16. (Color online) Top panel shows a sketch of current distribution in case of resistive electrodes and contact configuration for three- and four-probe measurements. The main panel shows simulated *I-V* curves in the three-probe (dashed lines) and four-probe (solid lines) configurations for different in-plane electrode resistances. It is seen that in-plane resistance distorts the measurement of junction characteristics and that acute back bending can develop in the four-probe case for high in-plane resistance. Inset shows the in-plane IVC.

exhibit acute back bending[71] and three-probe measurements that do not.

The top panel in Fig. 16 shows a sketch of the mesa structure. The current I is biased through the top electrode and returned through the crystal, which serves as the bottom electrode. The voltage can be measured either in four-probe V_{4p} or three-probe V_{3p} configuration, as shown in the figure.

If electrodes (both top and bottom) are resistive, then there is a voltage gradient along the electrodes and the bias current is distributed nonuniformly within the mesa, as shown by thin vertical arrows. Let $R_{1,2}$ be the in-plane resistance of top and bottom electrodes within the mesa area $0>x>a$ and R_c be the c-axis resistance of the mesa itself. Following Ref. 59, the current and voltage distributions in this case can be described by the following system of equations:

$$\frac{dV_1}{dx} = -\frac{R_1}{a} I_1,$$

$$\frac{dV_2}{dx} = -\frac{R_2}{a} I_2,$$

$$I_1(x) + I_2(x) = I,$$

$$V_1(x) - V_2(x) = -R_c a \frac{dI_1}{dx},$$

with boundary conditions $I_1(0)=I$ and $I_1(a)=0$.

In the four-probe configuration, the measured voltage is $V_{4p}=V_1(a)-V_2(0)$, which yields

$$V_{4p} = \frac{IR_1R_2}{(R_1+R_2)\alpha}\left[\frac{\left(\frac{R_1}{R_2}+\frac{R_2}{R_1}+2\cosh\alpha\right)}{\sinh\alpha} - \alpha\right], \quad \text{(B1)}$$

where $\alpha=\sqrt{\frac{R_1+R_2}{R_c}}$. In case $R_1=R_2$ it coincides with the result of Ref. 59.

In the three-probe configuration the measured voltage is $V_{3p}=V_1(0)-V_2(0)$, which yields

$$V_{3p} = \frac{I}{\alpha}\left[\frac{R_2+R_1\cosh\alpha}{\sinh\alpha}\right]. \quad \text{(B2)}$$

The main panel in Fig. 16 shows calculated four-probe (solid lines) and three-probe (dashed lines) IVCs for the case of identical superconducting electrodes $R_1=R_2=R_{ab}(I)$ with the in-plane critical current I_c^{ab} and the IVC as shown in the inset. For $R_{ab}=0$ the measured IVC coincides with real c-axis IVC of the mesa. But substantial deviations occur when the bias current exceeds I_c^{ab} and electrodes become resistive.

For the case of Bi-2212 mesas, R_1 is the resistance of the top gold electrode (typically negligible) and R_2 is the nonlinear ab-plane resistance of the CuO plane beneath the mesa (with the IVC sketched in the inset of Fig. 16). As will be shown below, the latter is non-negligible.

2. Limitations on the mesa size

I want to emphasize that large mesas may not be suitable for ITS even in the absence of self-heating. To probe the gap, one should be able to reach the sum-gap voltage, $V_{sg}\sim 60$ meV per IJJ, without loosing the equipotentiality of the bottom CuO plane, which is used as the return current lead and the second voltage electrode.

Let us estimate the maximum mesa size, suitable for ITS, in the absence of self-heating. Consider a square mesa with the in-plane size a. The bias current required for reaching the sum-gap voltage is $I_{sg}\simeq V_{sg}/(\rho_c s/a^2)$, where $\rho_c\simeq 30\ \Omega$ cm is the c-axis tunnel (large bias) resistivity and $s\simeq 1.5$ nm is the interlayer spacing. This current is flowing through the perimeter of the last IJJ into the bottom CuO layer and should not exceed the in-plane critical current of that layer. Provided the in-plane critical current density is $J_c^{ab}\sim 10^7$ A/cm^2,[71] the in-plane critical current of the bottom CuO plane through the perimeter of the mesa is $\sim 4J_c^{ab}sa$. Therefore, the mesa size should be smaller than $a_{\max}\simeq 4J_c^{ab}s^2\rho_c/V_{sg}\simeq 4.5\ \mu$m. Thus, miniaturization is essential for ITS. Otherwise the return current and voltage contacts are no longer equipotential, leading to the negative measured differential resistance in the four-probe configuration, as shown in Fig. 16.

To cause a substantial distortion, the total in-plane resistance should be larger than the mesa resistance. Let us see if this is the case for Bi-2212. The in-plane resistance of the bottom CuO plane in the square $a \times a$ is

$$R_{2,ab}(\square) = \rho_{ab} a/sa \sim 10^{-4}(\Omega\ \mathrm{cm})/1.5(\mathrm{nm}) = 667(\Omega).$$

The c-axis mesa resistance is $R_c = \rho_c Ns/a^2 \sim 30\ (\Omega\ \mathrm{cm})1.5\ (\mathrm{nm})N/a^2 = 450N/[a(\mu\mathrm{m})]^2(\Omega)$.

For a mesa $5 \times 5\ \mu\mathrm{m}^2$ with $N=10$ IJJs, $R_c = 180\ \Omega$ is about four times smaller than $R_{2,ab}(\square)$. Thus we see that distortion by in-plane resistance can indeed be significant for larger mesas with a small number of junctions.

The proposed model explains why four- and three-probe measurements of Bi-2212 mesas may be very different. From Fig. 16 it is seen that four- and three-probe measurements respond differently to in-plane resistivity. In the three-probe case, it just leads to appearance of an additional series resistance. But in the four-probe configuration it may lead to development of the acute back bending, precluding any spectroscopic analysis.

The model may also explain a strange behavior of mesas with very small amount of junctions.[72] From the estimations above it follows that, for a mesa $5 \times 5\ \mu\mathrm{m}^2$ with only one IJJ the in-plane resistance is about 40 times larger than the mesa resistance, which makes such mesas extremely prone to distortion by in-plane resistance and, probably, not suitable for ITS.

*vladimir.krasnov@fysik.su.se

[1] H. Ding, J. R. Engelbrecht, Z. Wang, J. C. Campuzano, S. C. Wang, H. B. Yang, R. Rogan, T. Takahashi, K. Kadowaki, and D. G. Hinks, Phys. Rev. Lett. **87**, 227001 (2001).

[2] W. S. Lee, I. M. Vishik, K. Tanaka, D. H. Lu, T. Sasagawa, N. Nagaosa, T. P. Devereaux, Z. Hussain, and Z. X. Shen, Nature (London) **450**, 81 (2007); T. Kondo, T. Takeuchi, A. Kaminski, S. Tsuda, and S. Shin, Phys. Rev. Lett. **98**, 267004 (2007).

[3] K. Tanaka, W. S. Lee, D. H. Lu, A. Fujimori, T. Fujii, Risdiana, I. Terasaki, D. J. Scalapino, T. P. Devereaux, Z. Hussain, and Z. X. Shen, Science **314**, 1910 (2006).

[4] A. Damascelli, Z. Hussain, and Z. X. Shen, Rev. Mod. Phys. **75**, 473 (2003).

[5] Ch. Renner, B. Revaz, J. Y. Genoud, K. Kadowaki, and O. Fischer, Phys. Rev. Lett. **80**, 149 (1998).

[6] A. N. Pasupathy, A. Pushp, K. K. Gomes, C. V. Parker, J. S. Wen, Z. J. Xu, G. D. Gu, S. Ono, Y. Ando, and A. Yazdani, Science **320**, 196 (2008).

[7] S. Misra, S. Oh, D. J. Hornbaker, T. DiLuccio, J. N. Eckstein, and A. Yazdani, Phys. Rev. Lett. **89**, 087002 (2002).

[8] R. Kleiner and P. Müller, Phys. Rev. B **49**, 1327 (1994).

[9] V. M. Krasnov, N. Mros, A. Yurgens, and D. Winkler, Phys. Rev. B **59**, 8463 (1999).

[10] Yu. I. Latyshev, A. E. Koshelev, V. N. Pavlenko, M. B. Gaifulin, T. Yamashita, and Y. Matsuda, Physica C **367**, 365 (2002).

[11] S. M. Kim, H. B. Wang, T. Hatano, S. Urayama, S. Kawakami, M. Nagao, Y. Takano, T. Yamashita, and K. Lee, Phys. Rev. B **72**, 140504(R) (2005).

[12] H. B. Wang, P. H. Wu, and T. Yamashita, Phys. Rev. Lett. **87**, 107002 (2001).

[13] V. M. Krasnov, T. Bauch, and P. Delsing, Phys. Rev. B **72**, 012512 (2005).

[14] K. Inomata, S. Sato, K. Nakajima, A. Tanaka, Y. Takano, H. B. Wang, M. Nagao, H. Hatano, and S. Kawabata, Phys. Rev. Lett. **95**, 107005 (2005).

[15] Yu. I. Latyshev, S. J. Kim, V. N. Pavlenko, T. Yamashita, and L. N. Bulaevskii, Physica C **362**, 156 (2001).

[16] S. Ooi, T. Mochiku, and K. Hirata, Phys. Rev. Lett. **89**, 247002 (2002).

[17] For a review, see, e.g., J. P. Carbotte, Rev. Mod. Phys. **62**, 1027 (1990).

[18] J. L. Tallon and J. W. Loram, Physica C **349**, 53 (2001).

[19] R. Huebener, Supercond. Sci. Technol. **8**, 189 (1995).

[20] I. L. Landau and H. R. Ott, J. Low Temp. Phys. **139**, 175 (2005); Phys. Rev. B **66**, 144506 (2002).

[21] M. J. Naughton, Phys. Rev. B **61**, 1605 (2000).

[22] B. Rosenstein, B. Y. Shapiro, R. Prozorov, A. Shaulov, and Y. Yeshurun, Phys. Rev. B **63**, 134501 (2001); Fareh Pei-Jen Lin and B. Rosenstein, *ibid.* **71**, 172504 (2005).

[23] F. Bouquet, L. Fruchter, I. Sfar, Z. Z. Li, and H. Raffy, Phys. Rev. B **74**, 064513 (2006); Y. Ando, G. S. Boebinger, A. Passner, L. F. Schneemeyer, T. Kimura, M. Okuya, S. Watauchi, J. Shimoyama, K. Kishio, K. Tamasaku, N. Ichikawa, and S. Uchida, *ibid.* **60**, 12475 (1999).

[24] Y. Wang, L. Li, M. J. Naughton, G. D. Gu, S. Uchida, and N. P. Ong, Phys. Rev. Lett. **95**, 247002 (2005); Y. Wang, L. Li, and N. P. Ong, Phys. Rev. B **73**, 024510 (2006).

[25] G. Deutscher, Nature (London) **397**, 410 (1999).

[26] M. Itoh, S. I. Karimoto, K. Namekawa, and M. Suzuki, Phys. Rev. B **55**, R12001 (1997); M. Suzuki and T. Watanabe, Phys. Rev. Lett. **85**, 4787 (2000).

[27] V. M. Krasnov, A. Yurgens, D. Winkler, P. Delsing, and T. Claeson, Phys. Rev. Lett. **84**, 5860 (2000).

[28] V. M. Krasnov, Phys. Rev. B **65**, 140504(R) (2002).

[29] M. LeTacon, A. Sacuto, A. Georges, G. Kotliar, Y. Gallais, D. Colson, and A. Forget, Nat. Phys. **2**, 537 (2006).

[30] Y. Wang and H. H. Wen, EPL **81**, 57007 (2008); H. Gao, C. Ren, L. Shan, Y. Wang, Y. Z. Zhang, S. P. Zhao, X. Yao, and H. H. Wen, Phys. Rev. B **74**, 020505(R) (2006).

[31] V. J. Emery, S. A. Kivelson, and O. Zachar, Phys. Rev. B **56**, 6120 (1997).

[32] J. Zaanen and B. Hosseinkhani, Phys. Rev. B **70**, 060509(R) (2004); C. M. Varma, *ibid.* **73**, 155113 (2006); S. Sachdev, Nat. Phys. **4**, 173 (2008).

[33] Z. Tesanovic, Nat. Phys. **4**, 408 (2008).

[34] V. J. Emery and S. A. Kivelson, Nature (London) **374**, 434 (1995); A. K. Nguyen and A. Sudbo, Phys. Rev. B **60**, 15307 (1999).

[35] For a review, see, e.g., A. I. Larkin and A. A. Varlamov, *Theory of Fluctuations in Superconductors* (Oxford University Press, New York, 2009).

[36] D. B. Haviland, Y. Liu, and A. M. Goldman, Phys. Rev. Lett. **62**,

2180 (1989); Y. M. Strelniker, A. Frydman, and S. Havlin, Phys. Rev. B **76**, 224528 (2007); for a review, see, e.g., I. S. Beloborodov, A. V. Lopatin, V. M. Vinokur, and K. B. Efetov, Rev. Mod. Phys. **79**, 469 (2007).

[37] N. Doiron-Leyraud, C. Proust, D. LeBoeuf, J. Levallois, J. B. Bonnemaison, R. X. Liang, D. A. Bonn, W. N. Hardy, and L. Taillefer, Nature (London) **447**, 565 (2007); E. A. Yelland, J. Singleton, C. H. Mielke, N. Harrison, F. F. Balakirev, B. Dabrowski, and J. R. Cooper, Phys. Rev. Lett. **100**, 047003 (2008).

[38] S. O. Katterwe, A. Rydh, and V. M. Krasnov, Phys. Rev. Lett. **101**, 087003 (2008).

[39] Y. Yamada, K. Anagawa, T. Shibauchi, T. Fujii, T. Watanabe, A. Matsuda, and M. Suzuki, Phys. Rev. B **68**, 054533 (2003).

[40] M. H. Bae, J. H. Park, J. H. Choi, H. J. Lee, and K. S. Park, Phys. Rev. B **77**, 094519 (2008).

[41] V. M. Krasnov, Phys. Rev. Lett. **97**, 257003 (2006).

[42] A. Yurgens, D. Winkler, T. Claeson, S. Ono, and Y. Ando, Phys. Rev. Lett. **90**, 147005 (2003).

[43] K. Schlenga, R. Kleiner, G. Hechtfischer, M. Mößle, S. Schmitt, P. Müller, Ch. Helm, Ch. Preis, F. Forsthofer, J. Keller, H. L. Johnson, M. Veith, and E. Steinbeiß, Phys. Rev. B **57**, 14518 (1998).

[44] O. S. Chana, A. R. Kuzhakhmetov, P. A. Warburton, D. M. C. Hyland, D. Dew-Hughes, C. R. M. Grovenor, R. J. Kinsey, G. Burnell, W. E. Booij, M. G. Blamire, R. Kleiner, and P. Muller, Appl. Phys. Lett. **76**, 3603 (2000).

[45] M. Nagao, S. Urayama, S. M. Kim, H. B. Wang, K. S. Yun, Y. Takano, T. Hatano, I. Iguchi, T. Yamashita, M. Tachiki, H. Maeda, and M. Sato, Phys. Rev. B **74**, 054502 (2006).

[46] T. Nachtrab, D. Koelle, R. Kleiner, C. Bernhard, and C. T. Lin, Phys. Rev. Lett. **92**, 117001 (2004).

[47] V. M. Krasnov, A. E. Kovalev, A. Yurgens, and D. Winkler, Phys. Rev. Lett. **86**, 2657 (2001).

[48] Yu. I. Latyshev, P. Monceau, S. Brazovskii, A. P. Orlov, and T. Fournier, Phys. Rev. Lett. **96**, 116402 (2006).

[49] T. Nachtrab, S. Heim, M. Mossle, R. Kleiner, R. Koch, O. Waldmann, P. Muller, T. Kimura, and Y. Tokura, Phys. Rev. B **65**, 012410 (2001).

[50] K. Lee, W. Wang, I. Iguchi, M. Tachiki, K. Hirata, and T. Mochiku, Phys. Rev. B **61**, 3616 (2000); M. B. Gaifullin, Y. Matsuda, N. Chikumoto, J. Shimoyama, K. Kishio, and R. Yoshizaki, Physica C **362**, 228 (2001).

[51] A. Yurgens, D. Winkler, N. V. Zavaritsky, and T. Claeson, Phys. Rev. Lett. **79**, 5122 (1997).

[52] V. M. Krasnov, M. Sandberg, and I. Zogaj, Phys. Rev. Lett. **94**, 077003 (2005).

[53] V. M. Krasnov, T. Bauch, S. Intiso, E. Hurfeld, T. Akazaki, H. Takayanagi, and P. Delsing, Phys. Rev. Lett. **95**, 157002 (2005).

[54] V. M. Krasnov, T. Golod, T. Bauch, and P. Delsing, Phys. Rev. B **76**, 224517 (2007).

[55] N. Morozov, L. Krusin-Elbaum, T. Shibauchi, L. N. Bulaevskii, M. P. Maley, Y. I. Latyshev, and T. Yamashita, Phys. Rev. Lett. **84**, 1784 (2000).

[56] S. P. Zhao, X. B. Zhu, Y. F. Wei, G. H. Chen, Q. S. Yang, and C. T. Lin, Phys. Rev. B **72**, 184511 (2005).

[57] P. J. Thomas, J. C. Fenton, G. Yang, and C. E. Gough, Physica C **341-348**, 1547 (2000); J. C. Fenton, P. J. Thomas, G. Yang, and C. E. Gough, Appl. Phys. Lett. **80**, 2535 (2002).

[58] H. B. Wang, S. Guenon, J. Yuan, A. Iishi, S. Arisawa, T. Hatano, T. Yamashita, D. Koelle, and R. Kleiner, Phys. Rev. Lett. **102**, 017006 (2009).

[59] I. Giaever, *Tunneling Phenomena in Solids*, edited by E. Bursein and S. Lundquist (Plenum Press, New York, 1969), p. 19.

[60] V. M. Krasnov, A. Yurgens, D. Winkler, and P. Delsing, J. Appl. Phys. **89**, 5578 (2001).

[61] At low enough dissipation powers, the $\log[dI/dV(V)]$ curves were V-shape-like for all crystals studied here. Most clearly it appears in slightly underdoped crystals, as shown in Fig. 4. Certain doping-dependent distortion to the V shape occurs both with underdoping and overdoping, as can be seen from Fig. 5(b).

[62] V. M. Krasnov, Physica C **372-376**, 103 (2002).

[63] D. Vion, M. Gotz, P. Joyez, D. Esteve, and M. H. Devoret, Phys. Rev. Lett. **77**, 3435 (1996).

[64] A. Franz, Y. Koval, D. Vasyukov, P. Muller, H. Schneidewind, D. A. Ryndyk, J. Keller, and C. Helm, Phys. Rev. B **69**, 014506 (2004); P. A. Warburton, A. R. Kuzhakhmetov, O. S. Chana, G. Burnell, M. G. Blamire, H. Schneidewind, Y. Koval, A. Franz, P. Müller, D. M. C. Hyland, D. Dew-Hughes, H. Wu, and C. R. M. Grovenor, J. Appl. Phys. **95**, 4941 (2004).

[65] For a recent overview of CDW/SDW scenario of the PG, see, e.g., T. Ekino, A. M. Gabovich, M. S. Li, M. Pekala, H. Szymczak, and A. I. Voitenko, J. Phys.: Condens. Matter **20**, 425218 (2008).

[66] V. N. Zavaritsky, Phys. Rev. Lett. **92**, 259701 (2004); Physica C **404**, 440 (2004); Phys. Rev. B **72**, 094503 (2005).

[67] V. M. Krasnov, Phys. Rev. B **75**, 146501 (2007).

[68] A. Yurgens, D. Winkler, T. Claeson, S. Ono, and Y. Ando, Phys. Rev. Lett. **92**, 259702 (2004); arXiv:cond-mat/0309131 (unpublished).

[69] H. B. Wang, T. Hatano, T. Yamashita, P. H. Wu, and P. Müller, Appl. Phys. Lett. **86**, 023504 (2005).

[70] M. F. Crommie and A. Zettl, Phys. Rev. B **43**, 408 (1991).

[71] L. X. You, A. Yurgens, and D. Winkler, Phys. Rev. B **71**, 224501 (2005).

[72] L. X. You, M. Torstensson, A. Yurgens, D. Winkler, C. T. Lin, and B. Liang, Appl. Phys. Lett. **88**, 222501 (2006).